

Use Authorization

In presenting this thesis in partial fulfillment of the requirements for an advanced degree at Idaho State University, I agree that the Library shall make it freely available for inspection. I further state that permission to download and/or print my thesis for scholarly purposes may be granted by the Dean of the Graduate School, Dean of my academic division, or by the University Librarian. It is understood that any copying or publication of this thesis for financial gain shall not be allowed without my written permission.

Signature _____

Date _____

Micro-Computed Tomography Analysis of Developing *Carollia*
perspicillata & Interdigital Expression of *Cyp26b1*, a Potential Digit
Patterning Gene

by

Aaron Harnsberger

A thesis submitted in partial fulfillment of the requirements for the degree of

Master of Science in the Department of Biological Sciences

Idaho State University

Summer 2016

Copyright (2016) Aaron Harnsberger

Committee Approval

To the Graduate Faculty:

The members of the committee appointed to examine the thesis of Aaron Harnsberger find it satisfactory and recommend that it be accepted.

Curt Anderson, PhD
Major Advisor

Jean Pfau, PhD
Co-Advisor

Richard Behringer, PhD
Committee Member

Susan Mackem, MD, PhD
Committee Member

Wayne Gabardi, PhD
Graduate Faculty Representative

Idaho State UNIVERSITY

Office for Research Integrity
921 South 8th Avenue, Stop 8046 • Pocatello, Idaho 83209-8046

March 8, 2016

Curtis Anderson, Ph.D.
Mail Stop 8007
Biological Sciences
Pocatello, Id 83209

RE: Your application dated 2/22/2016 regarding study number 741: Neurotransmitters in the developing brainstem of the bullfrog, *Rana catesbiana*

Dear Dr. Anderson:

Your request for approval of the new protocol listed above was reviewed at the 3/8/2016, meeting of the Idaho State University IACUC. This is to confirm that your protocol was approved. Your protocol number is 741.

You are free to proceed with your study as described in your protocol effective immediately.

The study is subject to annual review on or before 3/8/2017, unless closed before that date.

Please note that any changes to the protocol as approved must be immediately reported and approved. Contact me (208-282-2179; fax 208-282-4723; email: anmlcare@isu.edu) if you have any questions or require further information.

Sincerely,

Tom Bailey
IACUC Coordinator

Dedication:

This thesis is dedicated to my family. Without their support I could not have done this.

Acknowledgements:

I would like to acknowledge the late Dr. Chris Cretkos for introducing, training, guiding and mentoring me in this field of research. He offered me a chance to begin working on this project, and set me on the path that was followed to get here. I would also like to acknowledge Dr. Richard Behringer for joining my committee and giving me the opportunity to work with the data presented here. He invited me to make the collection trips to Trinidad and helped train me in collecting bats and embryos. Dr. Susan Mackem also joined my committee and provided me with data used here. She was helpful in many aspects of my project, especially when examining genetic expression in embryos. Dr. Jean Pfau was a member of my committee and then became my primary advisor after Chris passed away and I would not be here without her. She was always there to keep me on track and working towards a stated goal in my project. Dr. Curt Anderson was the only person who started and finished with me at Idaho State University. He was on my committee from the first day to the last and was always a positive force. I also want to acknowledge Dr. Mark Austin for helping with the administrative problems that arose, as well as setting up a new animal protocol to keep me working.

Table of Contents:

List of Illustrations	ix
List of Figures	x
List of Tables	xiii
List of Abbreviations	xiv
Abstract	xvi
Chapter I:	
Introduction/Background	1
Chapter II: Methods	
Animals	10
Bat Embryo Preparations	10
Scanning	12
Riboprobe Synthesis	14
Whole-Mount <i>in situ</i> Hybridization	19
Chapter III: Results	
External micro-CT	21
Internal micro-CT	34
Forelimb micro-CT	40
Whole-mount <i>in situ</i> Hybridization	50
Chapter IV:	
Discussion	59
Future Research Possibilities & Inquiries	66
References	67
Appendix.....	70

List of Illustrations:

Illustration 1: Page 9. Location of the apical ectodermal ridge (AER) and zone of polarizing activity (ZPA) within the developing limb bud of bats.

List of Figures:

Figure 1: Page 22. Surface renderings of CS11 – 14 *Carollia perspicillata* embryos from micro-computed tomography, showing external morphologies. A – D are CS11. E – H are CS12. I – L are CS13. M – P are CS14. A, E, I & M are sagittal views. B, F, J & N are coronal views. C, G, K & O are cephalic dorsal views. D, H, L & P are caudal dorsal views. Open white arrow in A indicates optic vesicle. Open white arrow in F and H indicates forelimb buds. Open white arrow in I, J and L indicates hind limb buds. Open black arrow in I indicates otic vesicle. Closed white arrow in I indicates optic cup. Scale bar represents 0.5 mm. n = 1.

Figure 2: Page 24. Surface renderings of *Carollia perspicillata* embryos from micro-computed tomography, showing external morphologies. A – D are CS15. E – H are CS16. I – L are CS17. A, E & I are sagittal views. B, F & J are coronal views. C, G & K are cephalic dorsal views. D, H & L are caudal dorsal views. Open white arrow in A indicates nasal pit. Open white arrow in E indicates vibrissae. Scale bar represents 1 mm. n = 1.

Figure 3: Page 26. Surface renderings of *Carollia perspicillata* embryos from micro-computed tomography, showing external morphologies. A – D are CS18. E – H are CS19. I – L are CS20. A, E & I are sagittal views. B, F & J are coronal views. C, G & K are cephalic dorsal views. D, H & L are caudal dorsal views. Scale bar represents 1.5 mm. n = 1.

Figure 4: Page 28. Internal renderings of *Carollia perspicillata* embryos from micro-computed tomography, showing internal morphologies. Shown is a coronal slice, near midline, to view internal morphologies. A is CS11. B is CS12. C is CS13. Scale bar represents 0.5 mm. n = 1.

Figure 5: Page 30. Internal renderings of *Carollia perspicillata* embryos from micro-computed tomography, showing internal morphologies. Shown is a coronal slice, near midline, to view internal morphologies. A is CS14. B is CS15. C is CS16. Scale bar represents 1 mm. n = 1.

Figure 6: Page 32. Internal renderings of *Carollia perspicillata* embryos from micro-computed tomography, showing internal morphologies. Shown is a coronal slice, near midline, to view internal morphologies. A is CS17. B is CS18. Scale bar represents 1.5 mm. n = 1.

Figure 7: Page 35. Internal renderings of *Carollia perspicillata* embryos from micro-computed tomography, showing internal morphologies. Shown is a coronal slice, near midline, to view internal morphologies. A is CS19. B is CS20. Scale bar represents 2 mm. n = 1.

Figure 8: Page 37. Surface and internal renderings of *Carollia perspicillata* forelimbs from micro-computed tomography, showing developing forelimb morphologies. Dorsal (left column) and ventral (right column) views of the left CS15 forelimb, sectioned away from whole embryo. A & B show surface view. C & D show internal view. E & F show varied contrasts of internal view. Scale bar represents 0.5 mm. n = 1.

Figure 9: Page 39. Surface and internal renderings of *Carollia perspicillata* forelimbs from micro-computed tomography, showing developing forelimb morphologies. Dorsal (left column) and ventral (right column) views of the left CS16 forelimb, sectioned away from whole embryo. A & B show surface view. C & D show internal view. E & F show varied contrasts of internal view. Scale bar represents 0.5 mm. n = 1.

Figure 10: Page 41. Surface and internal renderings of *Carollia perspicillata* forelimbs from micro-computed tomography, showing developing forelimb morphologies. Dorsal (left column) and ventral (right column) views of the left CS17 forelimb, sectioned away from whole embryo. A & B show surface view. C & D show internal view. E & F show varied contrasts of internal view. Scale bar indicates 1 mm. n = 1.

Figure 11: Page 43. Surface and internal renderings of *Carollia perspicillata* forelimbs from micro-computed tomography, showing developing forelimb morphologies. Dorsal (left column) and ventral (right column) views of the left CS18 forelimb, sectioned away from whole embryo. A & B show surface view. C & D show internal view. E & F show varied contrasts of internal view. Scale bar represents 1 mm. n = 1.

Figure 12: Page 45. Surface and internal renderings of *Carollia perspicillata* forelimbs from micro-computed tomography, showing developing forelimb morphologies. Dorsal (left column) and ventral (right column) views of the left CS19 forelimb, sectioned away from whole embryo. A & B show surface view. C & D show internal view. E & F show varied contrasts of internal view. Scale bar represents 1.5 mm. n = 1.

Figure 13: Page 47. Surface and internal renderings of *Carollia perspicillata* forelimbs from micro-computed tomography, showing developing forelimb morphologies. Dorsal (left column) and ventral (right column) views of the left CS20 forelimb, sectioned away from whole embryo. A & B show surface view. C & D show internal view. E & F show varied contrasts of internal view. Scale bar represents 2 mm. n = 1.

Figure 14: Page 48. Digit lengths (mm) grouped in stages of development. Open bar is CS15. Spotted bar is CS16. Horizontal dashed bar is CS17. Checkered bar is CS18. Right-angled dashed bar is CS19. Left-angled dashed bar is CS20. n = 1.

Figure 15: Page 50. *Carollia perspicillata* *Cyp26b1* DNA sequence. Bold text indicated the start codon and stop codon. The grey text indicates the sequence of primers, and the area in between the primers indicates the sequence of the riboprobe.

Figure 16: Page 52. *Carollia perspicillata* CS15 whole-mount *in situ* hybridization expression of *Cyp26b1*. n = 1.

Figure 17: Page 54. *Carollia perspicillata* CS16 whole-mount *in situ* hybridization expression of *Cyp26b1*. A is CS16 Early. B is CS16. C is CS16 Late. n = 1 for each stage.

Figure 18: Page 56. Proximal to distal lengths of *Cyp26b1* expression in IDM area posterior to digits 2 and 3. Black bars are CS16E. White bars are CS16. Grey bars are CS16L. n = 1.

Figure 19: Page 57. Embryonic Day 12.5 mouse *Cyp26b1* expression. A shows the entire embryo and black box highlights area of focus. B is the close up of the forelimb to look at forelimb expression patterns. n = 1.

Figure 20: Page 58. *Carollia perspicillata* CS17 whole-mount *in situ* hybridization expression of *Cyp26b1*. n = 1.

List of Tables:

Table 1: Page 49. List of embryos used in micro-CT scans. 3 embryos from each stage were scanned. The highest quality scan of each stage was then chosen for the descriptions.

List of Abbreviations:

μ CT – Micro-computed tomography. 3D x-ray imaging on a small scale with high resolution.

μ m – Micrometer. 1 μ m is equal to 0.001 mm.

3D – Three dimensional. Image that has X, Y and Z axes.

AER – Apical ectodermal ridge. Thickening of tissue at the distal end of limb bud that serves as a signaling center for limb bud proliferation.

BCIP – 5-bromo-4-chloro-3-indolyl-phosphate. Reagent used in the final color reaction for whole-mount *in situ* hybridization.

cDNA – Complimentary deoxyribonucleic acid. Double stranded DNA that is reverse transcribed from a single stranded messenger RNA.

CS – *Carollia* stage. This is the staging system used for identifying timed tissues.

CS E – *Carollia* stage early. This is a refinement of a major stage based on an earlier, intermediate morphology.

CS L – *Carollia* stage late. This is a refinement of a major stage based on slightly more maturation of forelimb anatomy.

Cyp26b1 – Cytochrome P450 gene. This a gene that is translated into a retinoic acid metabolizing protein.

Cyp26b1 – Cytochrome P450 protein. This is a retinoic acid metabolizing protein that plays a role in chondrogenesis.

DNA – Deoxyribonucleic acid. This is the molecule that stores genetic information in the nucleus of most cell in an organism.

FGF – Fibroblast growth factor family. This gene family has 22 members.

Fgf8 – Fibroblast growth factor 8. This is gene known to play a role in forelimb growth.

HARP – This is software developed to analyze regional cardiac function.

IDM – Interdigital mesenchyme. This is the tissue between digit condensations that can influence anterior digit identity.

kb – Kilo bases. 1 kb is equal to 1000 nucleotides.

LB – Luria broth. This is a nutrient rich medium for growing bacteria.

ml – Milliliter. 1 ml is equal to 0.001 liters.

mm – Millimeter. 1 mm is equal to 0.001 meters.

mRNA – Messenger ribonucleic acid. This is a molecule that is transcribed from DNA and is translated to produce proteins.

NBT – Nitro blue tetrazolium. This is a reagent used in the final color reaction for whole-mount *in situ* hybridization.

NRRD – This is a file format that is recognized by 3D Slicer.

NTMT – Sodium-chloride-tris-magnesium Chloride-Tween 20. This is an alkaline phosphatase buffer used in whole-mount *in situ* hybridization.

PBS – This is a phosphate buffered saline solution used in whole-mount *in situ* hybridization.

PBT-H – This is PBS with 0.1% Tween 20 added.

PCR – Polymerase chain reaction. This is a technique used to duplicate small numbers of DNA, resulting in a higher magnitude of DNA.

pmole – Picomole. 1 pmole is equal to 0.000000000001 moles.

RNA-seq – Ribonucleic acid sequencing. This assay identifies the identity, presence and quantity of ribonucleic acids in tissue samples. Each sequence is related to a unique transcript.

Shh – Sonic hedgehog. This is a gene known to play a role in limb patterning.

SOC – Super Optimal broth with glucose added. This is a nutrient rich medium used for bacterial growth.

TIFF – This is an uncompressed image file type.

WISH – Whole-mount *in situ* hybridization. This is an assay that can be used to visualize gene expression in tissue.

ZPA – Zone of polarizing activity. This is an area in forelimbs that serves as a signaling center in anterior-posterior patterning.

Abstract:

The bat is a mammal with several similarities to mice, but with a unique forelimb morphology. This includes webbed wings that allow for powered flight. Little is known about the timing of differentiation of the forelimbs during development, or the sequence of genetic expression that leads to this unique forelimb. In order to address this, we scanned 10 developmental stages of *Carollia perspicillata*, a phyllostomid microbat, using micro-computed tomography and present an external view of these stages and look at the changing morphology. This included examination of the developmental morphology of the internal anatomy of *Carollia perspicillata*, and specifically both external and internal morphologies of the developing forelimb. These techniques were used together to identify developmental stages to use for whole-mount *in situ* hybridizations in order to examine the expression of the potential digit patterning gene, *Cyp26b1* in the developing forelimb. These methods led to identification of temporal and spatial expression of *Cyp26b1* in the bat. When compared to mouse, the expression pattern in the bat was spatially similar, although possible temporal differences were uncovered. Future studies are needed to identify other genes that influence the unique forelimb development of the bat.

Chapter I

Introduction/Background:

Developmental biology relies on using embryos at known stages of development to describe the processes that results in the mature animal. Staging of *Carollia perspicillata* (*C. perspicillata*) generated from timed matings of captive bred animals (Cretekos et al., 2005) brought this bat species into light as an appropriate developmental model. This paper showed stages of development that were younger than 40 days post conception (dpc) when the embryo was described as having an hourglass-shape. At this early stage the neural tube was just forming. The neural tube runs from the cephalic (head) end to the caudal (tail) end along the dorsal side of the developing embryo. The neural tube is the precursor to the central nervous system. Another significant feature observed at these early stages were somites. Somites run parallel to the neural tube on both the left and right sides. Somites are precursors to several tissues including skin, muscle, ribs and vertebrae.

At 40 dpc the embryos have developed forelimb buds. These forelimb buds protrude from the body of the embryo. They are initially composed of undifferentiated mesenchyme cells covered by an epithelium. Ultimately, the limb buds include progenitor cells for all the final tissues of the mature forelimb. This stage also displayed pharyngeal arches. These pharyngeal arches are located at the cephalic end on the ventral side of the embryo. Pharyngeal arches are precursors to auditory tissues, tonsils, the thymus, and jaw elements including the maxilla (upper jaw) and mandible (lower jaw). Otic and optic vesicles were also described at this stage. Vesicles are epithelial

invaginations that are precursors to the final structures. Otic vesicles will become the inner ear. Optic vesicles will become elements of the eye.

At 44 dpc nasal pits were described developing on the snout which will become the nostrils. At this point the initial growth that will become the proapatagium was also observed. The proapatagium is tissue that spans the gap from the neck to the wrist and runs anterior to the forelimb. The initial growth that will become the plagiopatagium is also present. The plagiopatagium is posterior to the forelimb and connects the gap from wrist to ankle. These precursors to patagia will be dermal membranes that increase surface area of the adult animal and contribute to powered flight and control.

By 50 dpc the paper describes digit condensations. These digit condensations are in the developing forelimb and are the initial cellular condensations that will undergo chondrogenesis. Chondrogenesis is the formation of cartilage, which will later become the bones and joints of the fingers. The tissue in between these digit condensations regress in other mammalian models, but in bats this tissue remains and becomes the dactylopatagium (interdigital webbing). Another growth of tissue was also described at this point in development. This outgrowth is located on the posterior side of the hind limb near the tail and is the precursor to the uropatagium. The uropatagium is tissue that spans from one ankle to tail. The bat presents a unique developmental model for studying embryonic development, especially in the highly adaptive forelimb.

The *C. perspicillata* embryonic staging system (Cretkos et al., 2005) has identified distinct landmarks in different stages, as well as morphological landmarks to help identify the staging of tissues. This allowed for using *C. perspicillata* in comparative studies with other developmental models. This staging system refers to

Carollia stages as CS and is denoted by a major stage in development. The staging system has provided information on distinct stages of bat development and we have carefully examined embryos to further distinguish both early (E) and late (L) periods within the major stages. An example of this is CS16E, which is a CS16 embryo that shows an earlier, intermediate morphology in forelimb development when compared to a CS16 embryo. These refinements of staging were performed by closely examining the limb morphology of the embryos and looking for evidence of slight, but recognizably distinct differences. These changes included small increases in limb length, the appearance of points at the distal tip of digit condensations, small recesses of dactylopatagia and slight changes in limb shape. This refinement of staging was performed to allow for narrower time points in development, as gene expression is very dynamic in a developing embryo. Besides these accepted staging methods there is not comprehensive morphological information on bat embryo development.

Bats are an interesting model for other reasons as well. They are a very diverse group of mammals. Bats can be insectivorous, frugivorous, nectivorous and hematophagic. Bats live in trees, caves, culverts, under bridges, and some are known to migrate. Besides the diversity within the group they are also the second most abundant group of mammals, after rodents. In some tropical regions bats are more numerous and diverse than rodents (Mayer et al. 2007). Despite their diversity, bats are a very specialized group of mammal in terms of physiological adaptations. They are the only mammal to achieve powered flight. Bats can echolocate and some species can enter torpor. There is also evidence that bats can delay the development of embryos after

implantation (Rasweiler IV & Badwaik, 1997). These characteristics make bats an appropriate candidate for use in different developmental research projects.

One study involving forelimb development showed *C. perspicillata* has some variation in the expression of a gene that plays a role in forelimb development. This was described in 2007, and it was found that *Fgf8*, a gene in the fibroblast growth factor (FGF) gene family, was expressed in an area that was 2.7 times wider than comparable stage mouse embryos (Cretokos, et al., 2007). This shows that even though genes are similar from one model to another, an expression difference may play a role in the final forelimb morphologies that we observe. *C. perspicillata* and *Miniopterus natalensis* show variation in the expression of another gene involved in forelimb development. Hockman, et al. (2008), found that *Sonic hedgehog* (*Shh*) expression was altered when compared to mouse at comparable stages. It was shown that the initial expression of *Shh* was delayed in bat embryos. When *Shh* expression was seen in the bat embryos the area of expression was larger. Another interesting finding was that there was a re-initiation of *Shh* expression in bat embryos that was not seen in mouse. The delay in initial expression, increased area of expression and second wave of expression in a gene that is known to play a role in forelimb development indicates that the regulation in genes plays a significant role in forelimb diversity.

Starting with initial limb bud outgrowth one of the signaling centers involved is the apical ectodermal ridge (AER). The induction of the AER results from *Fibroblast Growth factor* (*Fgf*) signaling that comes from the midline of the developing embryo (Casanova & Sanz-Ezquerro, 2007). The AER is located at the distal edge of the newly induced limb bud (Illustration 1). The AER appears as a thickening of the distal

ectoderm and it has been shown to express high amounts of *Fgf4* and *Fgf8* genes (Sun, Mariani, & Martin, 2002). The AER, in conjunction with the zone of polarizing activity (ZPA) are the primary signaling centers that drives production of limb outgrowth (Illustration 1).

The ZPA produces *Sonic hedgehog* (*Shh*), which has previously been described as being the primary signal for posterior digit identity. Digit identity includes overall length of digit, the number of phalanges and the number of joints. More recently it has been shown that *Shh* is not the only signal needed to achieve full digit identity (Dahn & Fallon, 2000, Sanz-Ezquerro & Tickle, 2003). It has been shown that digit identities, after *Shh* expression has ceased, are not fixed (Dahn & Fallon, 2000, Sanz-Ezquerro & Tickle, 2003). These final digit identities appear to be regulated by signals from their adjacent posterior interdigital mesenchymal (IDM) areas (Dahn & Fallon, 2000). Studying these IDM signals is critical in addressing the diversity of final digit morphologies seen throughout Mammalia.

An RNA-seq assay was performed using separate IDM areas from CS16 *C. perspicillata* embryos (Susan Mackem, personal communication). This data set showed differences in gene expression between each IDM area. Given the previous information it is likely that genes expressed differentially in these areas may play a role in the final digit identities observed in adult *C. perspicillata*. Given the truncated size of digit 2 when compared to digits 3 – 5, there may be genes variably expressed in the IDM directly posterior to digit 2 that plays a role in the unique identity.

One gene shown in the RNA-seq assay that was differentially expressed was *Cyp26b1*. *Cyp26b1* was shown to be expressed 1.5x higher in the IDM directly posterior

to digit 2 than in the IDM posterior to digit 1 and 2.2x higher than the IDMs posterior to digits 3 and 4. Showing an expression difference in the regions of interest during the stage of development that is thought to be critical in digit patterning makes *Cyp26b1* a potential candidate in the varying digit identities observed in adult *C. perspicillata*.

The *Cyp26b1* enzyme plays a role in retinoic acid signaling, and is known to degrade retinoic acid (Dranse, et al., 2011, Yashiro, et al., 2004). In a *Cyp26b1* knockout study, in which mice were genetically altered to not express the *Cyp26b1* transcript, the embryos had several malformations in skeletal elements, including major limb defects (Dranse, et al., 2011, Yashiro, et al., 2004). These defects included proximalization of the limbs, where the distal portion of the limbs did not develop and the limb was extremely truncated and malformed. The degradation of retinoic acid performed by *Cyp26b1* is thought to be critical in proximal-distal patterning and a preliminary step in chondrogenesis. Given the expression difference observed in the RNA-seq data at a critical stage for initial chondrogenesis in *C. perspicillata* forelimbs and the importance of the *Cyp26b1* enzyme in chondrogenesis events leads to further inquiry in the expression of *Cyp26b1* in the developing *C. perspicillata* forelimb. To identify stages of initial digit condensation near the IDM areas of interest we performed a micro-computed tomography assay.

Micro-computed tomography (μ CT) has been shown to be a powerful tool for embryonic imaging (Johnson et al., 2006, Kim, et al. 2011, Metscher, 2009, Paulus et al., 2000, Rennie et al., 2013, Wing et al. 2013). μ CT scans show a contrast difference when looking at mineralized tissues and soft tissues, as well contrast differences in different types of soft tissues. Dense or mineralized tissues appear light grey and white, while thin

tissue and hollow areas appear dark grey to black. μ CT scans can be performed at very fine resolution (3-50 μ m), and these scans can be achieved without any physical sectioning of the embryo. No physical sectioning results in all tissues being in the exact, undisturbed orientation that may otherwise be altered by traditional sectioning. The intact tissues also do not undergo any desiccation or shrinkage. Furthermore, the thickness of sections, location of sections, contrast, and intersecting sections can all be varied without the use of another embryo. Literature searches show different mammalian and non-mammalian embryos have been examined using μ CT, but in review of the literature it appears that whole bat embryos have yet to be examined (Johnson et al., 2006, Kim, et al. 2011, Metscher, 2009, Paulus et al., 2000, Rennie et al., 2013, Wing et al. 2013). Techniques developed for use on mouse embryos have been shown to work with bat embryos of similar size (data not shown). The presences of the CS staging system for the development of *C. perspicillata* embryos (Cretekos et al., 2005) allowing for use of both *C. perspicillata* staged embryos and μ CT to identify appropriate stages of limb development to use.

Whole-mount *in situ* hybridizations (WISH) assays have been used in conjunction with bat embryos to describe developmental gene expression for several years (Chen, et al., 2005, Cretekos et al. 2007, Cretekos et al. 2007, Hockman et al. 2008). WISH allows for locating mRNA transcripts in intact developing tissues. Using timed or staged tissues and WISH allows for identifying the spatial expression of genes and their patterns. Performing WISH on several stages of development leads to a temporal view of gene expression. Identifying expression of genes in particular tissue types at particular stages may indicate that the genes observed are contributing to the developmental processes

taking place Cretekos et al. 2007, Hockman et al. 2008. Using WISH to examine developing limbs, with particular genes thought to play a role in some part of the limb development process, is an accepted approach in identifying possible contributors in limb development from initial limb bud outgrowth to final developmental patterning.

In this study we will describe morphology of the developing *Carollia perspicillata* embryo with a focus on digit patterning using micro-computed tomography. We will test the hypothesis that the spatial pattern of a digit 2 patterning candidate gene is unique in bat when compared to mouse in an attempt to validate expression differences obtained in the RNA-seq assay.

In this study we used μ CT in parallel with WISH. This combination allowed us to first observe initial digit condensation when gene expression might first be seen and then use WISH to try and observe gene expression. We first show the μ CT assay with *C. perspicillata* embryos from CS10 - 20 developmental stages and describe some major external, morphological changes observed. We then look at CS11 – 20 coronal sections taken near the midline of the embryos, and highlight a few of the morphological changes observed. Next we examine forelimb development from CS15 – 20, with both external and internal views of distal forelimb development. Finally, we show the pattern of interdigital expression of *Cyp26b1*, a potential digit patterning gene in *C. perspicillata*. We compare the expression in bat to the expression in mouse. We do not see any unique expression patterns and visible expression is not sufficiently different to verify the RNA-seq data. However, whole-mount *in situ* hybridization uncovered possible temporal differences in expression between bat and mouse.

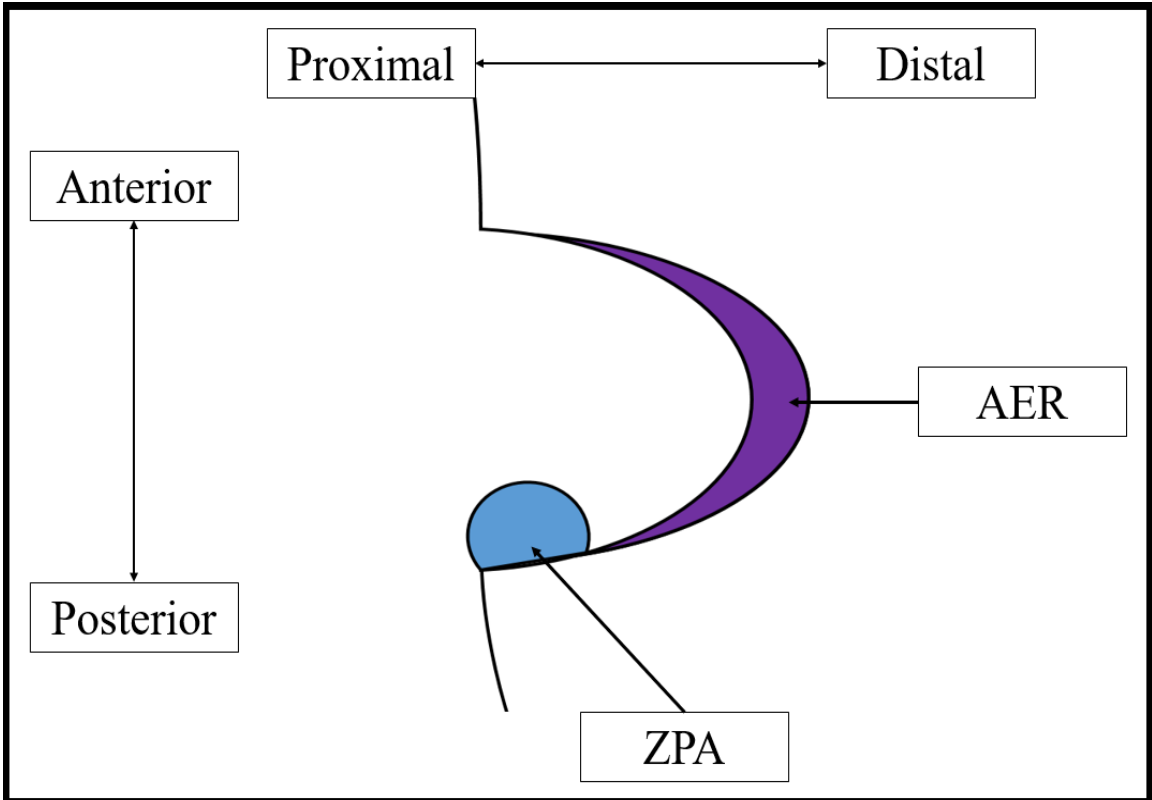


Illustration 1: Location of the apical ectodermal ridge (AER) and zone of polarizing activity (ZPA) within the developing limb bud of bats.

Chapter 2

Animals:

This study was performed using *C. perspicillata* embryos. All bats used for these studies were collected following the protocols described by Cretekos et al. (2009). Bats were collected from wild populations on the island of Trinidad. Collection trips were performed in either January or May to coincide with the known cycle of pregnancies in the population. Pregnant females were captured and transported to the Department of Life Sciences at the University of West Indies (UWI) in St. Augustine. The bats were collected and the embryos exported with permits obtained from the Wildlife Section of the Division of Forestry of Trinidad and Tobago.

Bat Embryo Preparation:

Bat embryos were collected, fixed and processed following Cretekos et al. (2009). Bats were euthanized by cervical dislocation. The reproductive tracts were dissected out and the embryos dissected from the uterus. The embryonic membranes were removed and the embryos were placed into 4°C 4% paraformaldehyde in phosphate buffered saline (PBS) overnight. The following day the embryos were rinsed twice in PBS followed by two 15 minute washes in PBS. The embryos were then dehydrated in 15 minute increments, starting with 25% methanol in PBS, followed by 50% methanol in PBS, 75% methanol in PBS and finally 2 consecutive washes in 100% methanol. These embryos were then stored at -80°C until used for these studies.

To prepare embryos for use after storage they were rehydrated in 15 minute increments starting with 75% methanol in PBS, followed by 50% methanol in PBS, 25%

methanol in PBS and two 15 minute washes in PBS. At this point embryos used for WISH were fully prepared. For μ CT the embryos were fixed longer by placing them back in 4°C 4% paraformaldehyde in PBS. CS11 – 16 (2 – 9.2 mm crown to rump length) embryos were left to fix overnight. Due to the larger size of the CS17 – 20 (10.1 – 17.1 mm crown to rump length) embryos, they were left in the 4°C 4% paraformaldehyde in PBS for 2 nights. The CS11 – 16 embryos were then placed directly in a 0.1N iodine solution at room temperature for 24 hours. The larger CS17 – 20 embryos went through an additional stabilization step in 4% paraformaldehyde, 4% acrylamide, 0.05% bis-acrylamide, 0.25% VA044 Initiator and 0.05% saponin in PBS and incubated at 4°C for 3 days. The CS17 – 20 embryos had all the air replaced with nitrogen in a desiccation chamber. These samples were placed in 37°C water for 3 hours. The gel around the samples was then peeled away. These stabilized embryos were placed in 0.1N iodine for 72 hours. These steps were performed following Wong, Spring & Henklmen (2013).

After the iodine immersion each sample was placed a 2 ml screw cap tube filled with melted 1% agarose. Forceps were used to position the embryos in the agarose as it cooled to get the best imaging position. These tubes were left to cool to room temperature before scanning.

Scanning:

Scanning was completed using 30 embryos, n=3 for each stage CS11 – 20.

Scanning was performed using the Skyscan 1272 (Bruker Corporation, Massachusetts) at the Baylor College of Medicine Optical Imaging Core (Houston, TX.). The camera rotation step was 0.300 degrees around the embedded embryo for each x-ray image taken. Frame averaging was used and set to 3. The pixel sizes used for image acquisition varied because the sizes of the embryos examined ranged from 2 mm – 17 mm when measured from crown to rump. CS11 & 12 pixel sizes are 3.0 μm . CS13 – 20 pixel sizes are 5 μm . Times for scans ranged from 1.5 hours to overnight depending on embryo stage.

The completed scans resulted in many TIFF x-ray images that were reconstructed into a 3D x-ray file using NRecon, version 1.6.9.8 (Bruker). Reconstructing the individual TIFF images into the 3D x-ray file ranged from 5 minutes to 75 minutes. The earlier staged embryos were smaller requiring less scan time while larger embryos at later stages required increasing scan times. Post processing to crop out the unused outer edges of each file and conversion to NRRD files were performed using HARP (Harmonic Phase Imaging).

The images retrieved from the scans were obtained using 3D Slicer (www.slicer.org). Within 3D Slicer there were several different modules used, including Volume, Volume Rendering, and Scene Selections. In order to annotate with correct scale bars each file had to be altered in the Volume module. This was performed by entering the correct scale of each file and re-centering the slicing panes. The Volume Rendering module was used to display and images the outer layers of the embryos in 3D.

This was performed by activating the module and altering contrasts until a desirable image was displayed. The Scene Selections module was used to capture each individual image used to make panels. This was performed by using the other modules to obtain a desirable image then switching over to the Scene Selections module and capturing the displayed image. Images were then saved as uncompressed TIFF files and used to make the panels shown.

Riboprobe Synthesis:

Synthesis of riboprobes that were specific to the *Cyp26b1* mRNA (messenger RNA) transcript required the use of *C. perspicillata* tissue to generate the appropriate cDNA (complimentary DNA). Forelimbs were dissected away from the embryo, homogenized using a flattened pipette tip to grind the tissue in a sterile 1.5 ml Eppendorf tube with QiAzol Lysis Reagent (Qiagen RNeasy Plus Universal Mini Kit (50) Cat. No. 73404). This mixture was then suctioned in and expelled from a 26-gauge hypodermic needle 10 times to ensure proper tissue homogenization. The Qiagen RNeasy Plus Universal Handbook (2010) was followed for the remaining steps. This resulted in isolated *C. perspicillata* RNA that was used for reverse transcription into cDNA.

The reverse transcription was completed following TaKaRa BluePrint 1st Strand cDNA Synthesis Kit protocol (2013). The isolated RNA was added to the provided buffer and solutions following the protocols, resulting in cDNA. This cDNA was quantitated using a Thermo Scientific NanoSpec.

Primers were designed using sequences from the RNA-seq assay. The *C. perspicillata Cyp26b1* sequence was compared to the *Cyp26b1* sequence of other bats to find areas of conservation (same DNA sequence between species) that were over 90% similar. Appropriate areas for primer locations had high similarity, roughly 50% guanine/cytosine content and 50% adenine/thymine content, and were around 20 nucleotides long. The forward primer was chosen from an area near the middle of the gene. The reverse primer was chosen from an area near the 3' end of the gene.

Polymerase chain reaction (PCR) was performed using 10 pmoles of the forward and reverse primers. 40 ng of cDNA were used. These were added to Bullseye Taq Reaction buffer with Thermo Scientific magnesium chloride.

The PCR product was immediately used in an electrophoresis assay to quantify the length of the nucleotide product. This was performed using a 2% agarose gel and Bullseye DNA loading buffer, which was added to the PCR product at the beginning of the electrophoresis to allow for visualization of the PCR product when the electrophoresis was complete. The PCR product length was determined using a Bulls eye 1 kb DNA ladder that was added immediately after the PCR product was placed in the gel.

After the electrophoresis an ultraviolet band was observed near the band in the 1 kb ladder that was equivalent to 700 nucleotides in length. This band was cut out of the agarose gel with a sterile razor blade and the PCR product was isolated from the gel. This was performed using Qiagen MinElute Gel Extraction Kit (Cat. No. 28604) and Quick Start Protocol (2011). The excised gel containing the PCR product was immersed in the supplied buffers and filtered to isolate the PCR product into a sterile 1.5 ml Eppendorf tube. This product was then sequenced on at the Molecular Research Core Facility in the Department of Biological Sciences at Idaho State University.

After verifying that the sequence was *Cyp26b1* using Nucleotide Blast (https://blast.ncbi.nlm.nih.gov/Blast.cgi?PAGE_TYPE=BlastSearch), the product was inserted into a bacterial plasmid vector (ligation). This was done using 50 ng of pGEM-T Easy Vector, Buffer, 4.5 µl of the PCR product and Promega T4 DNA Ligase. This

resulted in a bacterial plasmid that included the DNA sequence that was synthesized from PCR.

The ligated product was added to 50 μ l of competent *Escherichia coli* (*E. coli*) and left to rest in an ice bath for 20 minutes. The ligation reaction was then placed in a 42 °C water bath for 1 minute. The ligation reaction was then placed back into the ice bath for 1 minute. 500 μ l of Super Optimal broth with glucose (SOC) was added. These transformations were incubated for 30 minutes at 37 °C. 100 μ l of the transformation reactions were pipetted and spread onto a Luria broth (LB) agar plate treated with ampicillin. The plates were incubated at 37°C overnight.

Plates were observed the next morning and those with bacterial colony growth were used to pick individual colonies by touching the colony with sterile toothpicks. These toothpicks were placed in 3 ml liquid LB with ampicillin and placed in a 37°C chamber to incubate overnight. 1 ml of the 3 ml mixture was then centrifuged for 10 minutes. The LB was poured off and the bacterial growth remained as a pellet at the bottom.

This pellet of bacteria was then re-suspended in lysis solution and buffer and placed on ice for 10 minutes. The lysed bacterial cells were centrifuged for 10 minutes and the liquid supernatant was poured off leaving pelleted plasmids containing the DNA sequence of interest. This resulted in a small yield of plasmid that was sequenced at the Molecular Research Core Facility in the Department of Biological Sciences at Idaho State University.

After verifying the sequence 1 ml of the remaining 2 ml LB/bacterial mixture was pipetted into 100 ml of LB with ampicillin. This was placed in a 25°C chamber overnight.

The 100 ml mixture was centrifuged for 15 minutes and the liquid was poured off leaving a bacterial pellet. This pellet was re-suspended in Buffer P1 that was supplied with Qiagen CompactPrep Plasmid Midi Kit (25) (Cat. No. 12843) and the Quick-Start Protocol (2012) was followed. This resulted in a purified plasmid that was sequenced at the Molecular Research Core Facility in the Department of Biological Sciences at Idaho State University.

After verifying that the plasmid contained the desired *C. perspicillata Cyp26b1* gene restriction enzymes were used to linearize the plasmid. This was done using Thermo Scientific SPEI and SACII restriction enzymes. 5 µg of plasmid were added to 2 µl of restriction enzyme and 2 µl of buffer. These restriction reactions were left at room temperature overnight.

The linearization reactions were precipitated to remove all components of the reaction and leave the linear plasmid. This was done by adding 2 µl of 3M sodium acetate, 40 µl of ethanol and incubating at 80°C for 1 hour. The precipitation reactions were centrifuged for 10 minutes. The liquid was poured off and the linearized plasmid remained as a pellet at the bottom. This pellet was rinsed with 100 µl of 70% ethanol in water. The rinse was poured off and the pellet was air dried for 30 minutes. This pellet was re-suspended in 10 µl of water.

The linearized plasmid was then reacted with RNA polymerase enzymes and labeled nucleotides. The enzymes used were Fermentas SP6 and Thermo Scientific T7. The labeled nucleotides were Roche DIG RNA Labeling Mix. This reaction was performed following (Cretekos et al., 2009). This resulted in *C. perspicillata Cyp26b1* RNA that contained DIG labeled uracil in place of regular uracil. This was diluted in hybridization buffer at a concentration of 100 ng/ μ l of RNA in hybridization buffer. This concentrated riboprobe was stored at -20°C until use.

The concentrated riboprobe was diluted to 2 ng/ μ l in hybridization buffer for use in the WISH experiments. This was done by adding 40 μ l of concentrated riboprobe into 1.96 ml of hybridization buffer.

Whole-mount *in situ* Hybridization:

All steps for WISH were followed directly from Cretekos et al. (2009). The rehydrated embryos were permeabilized with 10ug/ml proteinase k in PBT-H (PBS with 0.1% Tween 20) for appropriate times listed for each stage. Superficial tissue times used were 20 minutes for CS15, 30 minutes for CS16E, 35 minutes for CS16, 40 minutes for CS16L and 50 minutes for CS17. The embryos were fixed after permeabilization in 4% paraformaldehyde in PBT-H for 20 minutes. The embryos were incubated at 65°C in the 2 ml of 2ng/μl riboprobe overnight.

Riboprobe was removed the following morning and the embryos were washed according to Cretekos et al. (2009). A blocking agent with Roche antiDIG AP-antibody was added and left to incubate at 4°C overnight. The following morning the embryos were rinsed and washed following Cretekos et al. (2009). This included 5 1 hour washes at room temperature and an overnight wash, all in Tris-Buffered Saline and 0.05% tween 20 (TBST).

The following morning the embryos were washed in an alkaline phosphatase buffer (NTMT). The embryos were then treated with 3.5 μl/ml 5-bromo-4-chloro-3-indolyl-phosphate (BCIP) and 4.5 μl/ml nitro blue tetrazolium (NBT) in NTMT. The embryos were washed in a dark container and agitated gently at room temperature for 15 minutes. The agitation was ceased and the embryos were given 15 minutes of incubation at room temperature. The development of color was sufficient at this point and the reaction was stopped by rinsing the embryos in PBT-H and fixing for 2 hours at room temp in 4% paraformaldehyde in PBT-H.

To image, the embryos were incubated in 50% glycerol in PBT-H at room temperature for 1 hour. A Leica MZ6 dissecting microscope and Leica DMC2900 camera were used for WISH image capture. WISH image scale bars and processing were done using Leica Application Suite Version 4.

Chapter 3

External micro-CT:

The use of *Carollia* for μ CT scans resulted in high resolution reconstructed images that can be manipulated to focus on anatomical features of interest. We focused first on overall, external morphological changes in the stages examined.

The CS11 embryo, collected in 2014, sample 133 (Fig. 1, A - D) exhibited the optic vesicle developing on the forebrain vesicle (open arrow in Fig. 1, A). There were two distinguishable pharyngeal arches. 22 pairs of somites were counted on this embryo. This varied from the number of somites observed in the staging of *C. perspicillata* in 2005 (Cretokos et al., 2005), in which 13 – 20 somites were found. The caudal end of the embryo was twisted around the trunk and protruded to the left. A face on view (Fig. 1, B) shows the twisting and protrusion.

The CS12 embryo, collected in 2010, sample 166 (Fig. 1, E - H) showed further development in the cephalic region. The 2 pharyngeal arches were closer together and the shape had changed when compared to the CS11 embryo. There were lateral thickenings and protrusions of the forelimbs (open arrows in Fig. 1, F & H). 26 pairs of somites were counted on this embryo. This count was consistent with the staging paper, which indicated 21 – 29 pairs of somites (Cretokos et al., 2005). The caudal end of the embryo was twisted and protruding to the left (Fig. 1, F).

The CS13 embryo, collected in 2014, sample 173 (Fig. 1, I-L) exhibited evidence of optic cups (solid arrow in Fig. 1, I), consistent with the staging of *C. perspicillata* (Cretokos, et al., 2005). The otic vesicles (hollow black arrow in Fig. 1, I) was also

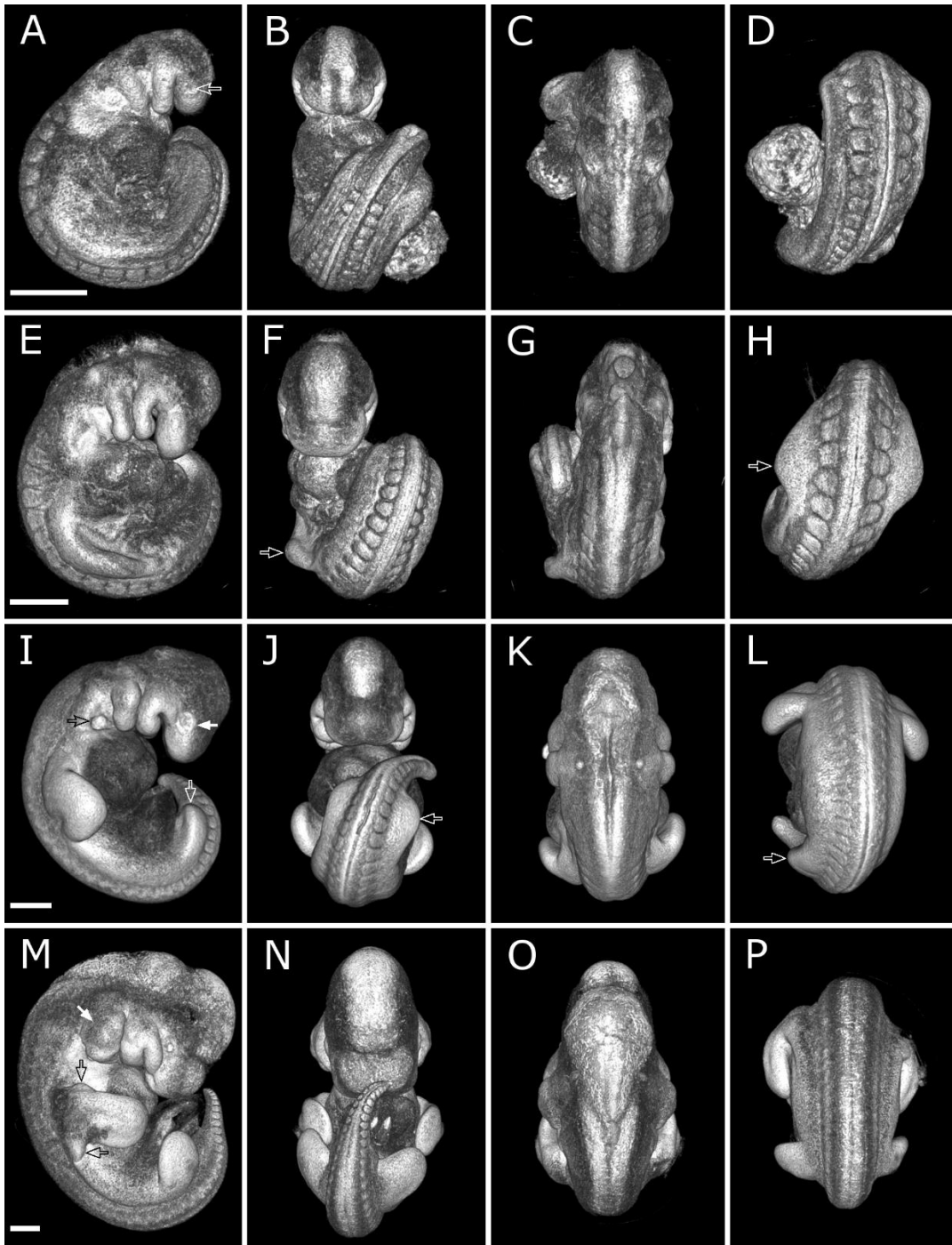


Figure 1: Surface renderings of CS11 – 14 *Carollia perspicillata* embryos from micro-computed tomography, showing external morphologies. A – D are CS11. E – H are CS12. I – L are CS13. M – P are CS14. A, E, I & M are sagittal views. B, F, J & N are coronal views. C, G, K & O are cephalic dorsal views. D, H, L & P are caudal dorsal views. Open white arrow in A indicates optic vesicle. Open white arrow in F and H indicates forelimb buds. Open white arrow in I, J and L indicates hind limb buds. Open black arrow in I indicates otic vesicle. Closed white arrow in I indicates optic cup. Scale bar represents 0.5 mm. n = 1.

present. The forelimb protrusions were very distinct and resembled a small paddle. Lateral thickenings were present where the hind limbs were beginning to develop (open arrows in Fig. 1, I, J & L). 32 somite pairs were counted, and this was consistent with the 30 – 35 somite pairs described in the staging of *C. perspicillata* (Cretekos et al., 2005). The twist to the left at the caudal end of the embryo still persisted (Fig. 1, J).

The CS14 embryo, collected in 2007, sample 070 (Fig. 1, M – P) had shape changes in the location of the previously described otic vesicle (solid arrow in Fig. 1, M). These changes were the initial formation of the pinnae. The pharyngeal arches showed signs of change. The first arch showed the maxillary and mandibular processes. The forelimbs resembled a longer paddle. There were 2 new dermal thickenings, one on the anterior and one on the posterior, of the medial portion of the forelimb (black, open arrows in Fig. 1, M). These thickenings may be the first evidence of the propatagium (tissue that spans shoulder to wrist) and plagiopatagium (tissue that spans wrist to ankle). The hind limb buds were paddle-like, yet still small (resembling the size and shape of forelimbs from previous stage). Somites were counted and there were 36 pairs present. This count was consistent with *C. perspicillata* staging (Cretekos et al., 2005), in which they described 36 – 40 somite pairs.

The CS15 embryo, collected in 2011, sample 199 (Fig. 2, A – D) showed the lens vesicle and optic cup. The pinnae were protruding more than the CS14 embryo (solid, black arrow in Fig. 2, A). Nasal pits were present on the snout (open, white arrow in Fig. 2, A). The forelimbs were longer (proximal to distal) and wider (anterior to posterior) (open, black arrows in Fig. 2, A). The patagia thickenings have expanded. The hind

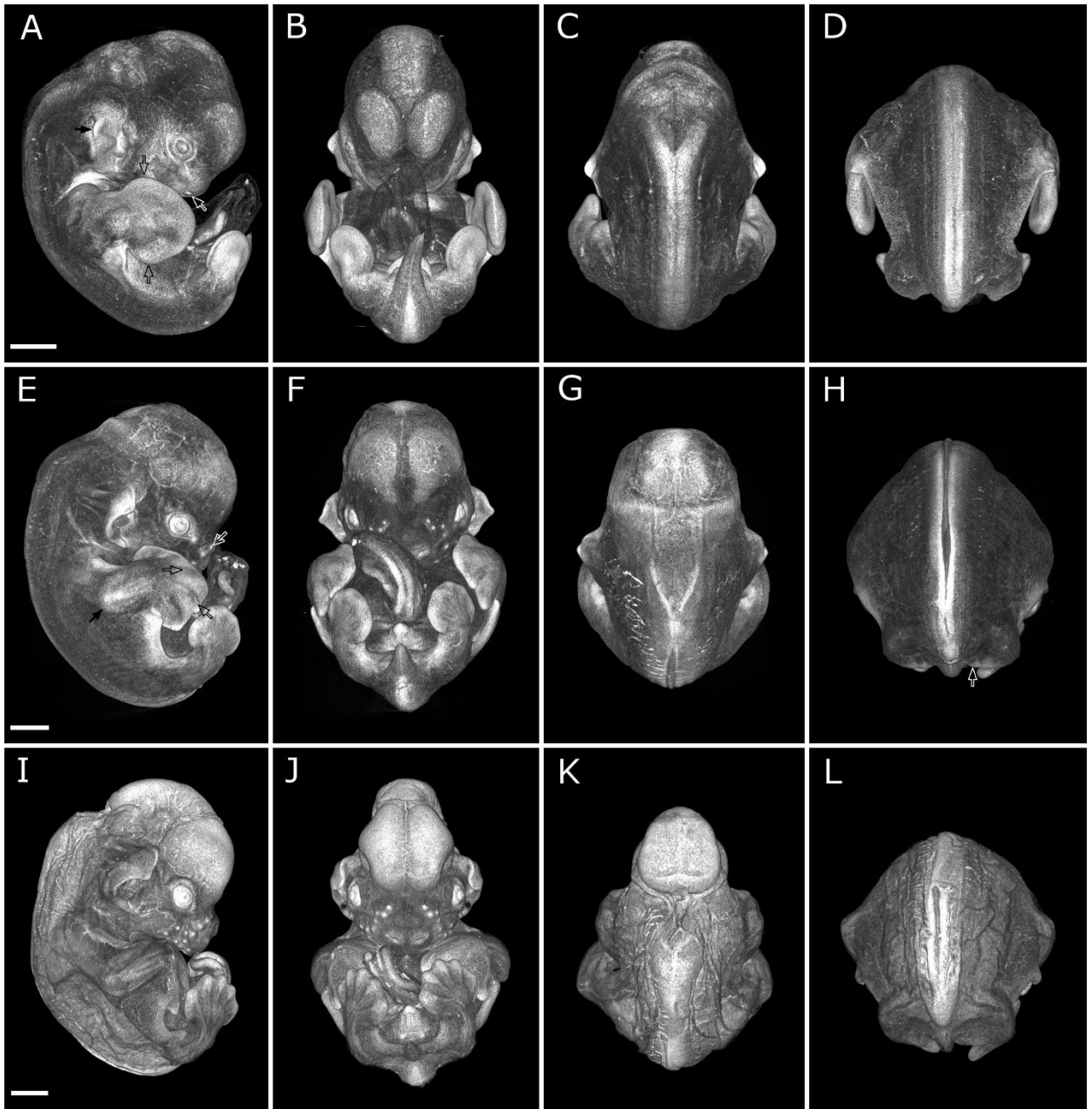


Figure 2: Surface renderings of *Carollia perspicillata* embryos from micro-computed tomography, showing external morphologies. A – D are CS15. E – H are CS16. I – L are CS17. A, E & I are sagittal views. B, F & J are coronal views. C, G & K are cephalic dorsal views. D, H & L are caudal dorsal views. Open white arrow in A indicates nasal pit. Open white arrow in E indicates vibrissae. Scale bar represents 1 mm. n = 1.

limb buds had changed shape, resembling a paddle. There were fewer somite pairs observed when compared to the CS14 embryo, indicating somitogenesis was complete. This was consistent with the *C. perspicillata* staging paper (Cretekos et al., 2005). The caudal portion of the embryo was no longer twisted around the trunk (Fig. 2, B).

The CS16 embryo, collected in 2007, sample 029 (Fig. 2, E – H) showed further development of the eye (Fig. 2, E & F). The tip of the pinnae began to curl and take on a shape of mature external ear (Fig. 2, E, F & G). This stage also showed further development of the face when compared to the CS15 embryo. This area protruded more and there were vibrissae (whisker follicles) arranged around the snout (open, white notched arrow in Fig. 2, E). The nostrils showed further definition (Fig. 2, F) when compared to the CS15 embryo. The forelimbs had changed shape and size when compared to the CS15 embryo. There was external evidence of digit condensations for digits 1 – 5 (open, black arrows in Fig. 2 E). This stage also showed further development in other parts of the forelimb including a bend in the limb indicating the development of upper, lower and elbow elements of the forelimb (solid, black arrow in Fig. 2, E). The width of the body at CS15 was 1.92 mm while the distal forelimb was 1.155 mm from the wrist to the distal tip of digit 3. CS16 showed an increase in body width to 2.165 mm and an increase in the distal forelimb to 1.212 mm from the wrists to the distal tip of digit 3. Both propatagium and plagiopatagium had grown out, distally from the body. The propatagium appeared to have expanded to connect from the base of digit 1 to the shoulder. The dactylopatagium (tissue that spans digit to digit) showed no evidence of regression in between the digits, but there was a protruding bump at the distal edge of digit 4. The overall shape change of the forelimb at this stage, along with the persisting

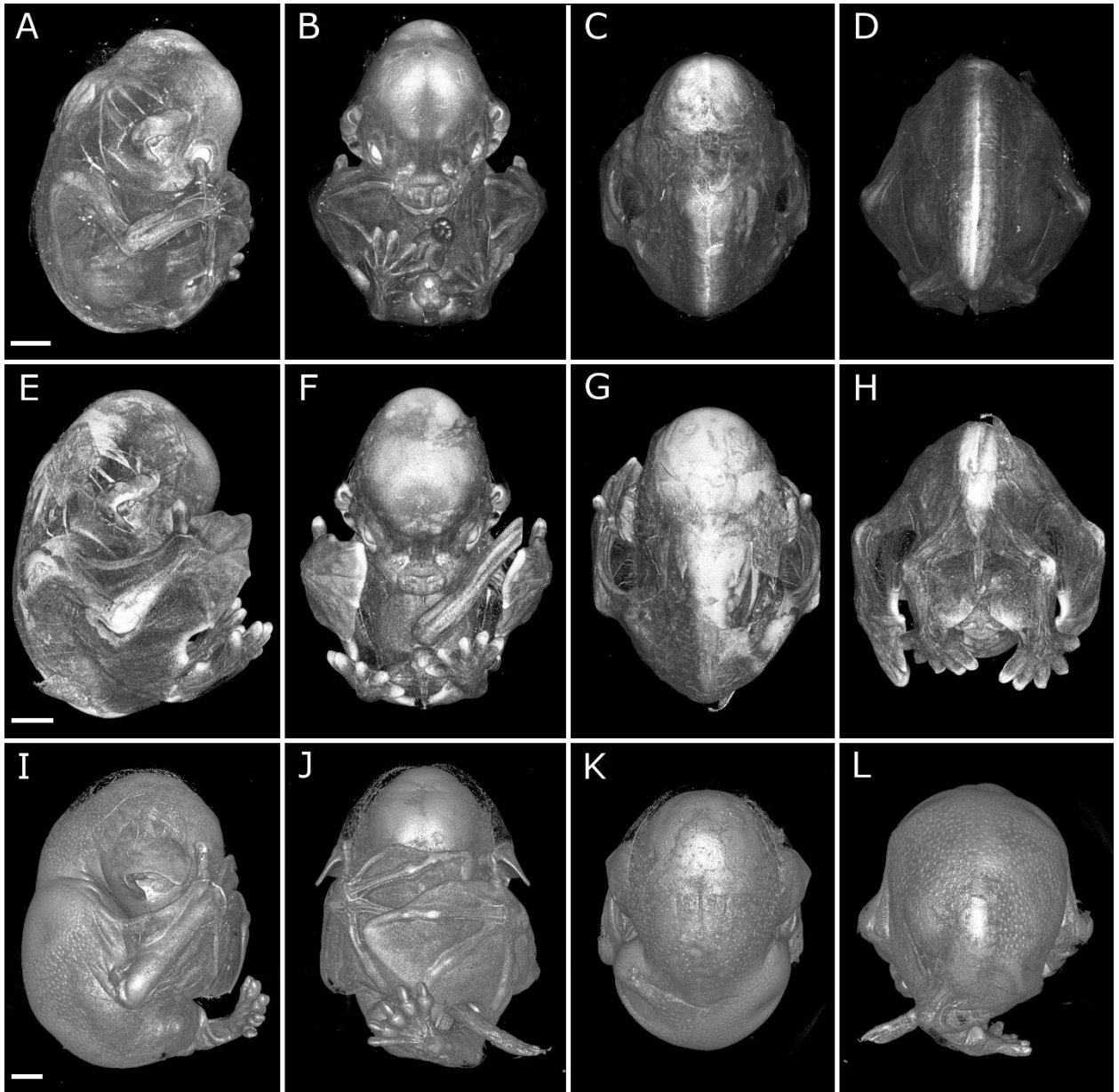


Figure 3: Surface renderings of *Carollia perspicillata* embryos from micro-computed tomography, showing external morphologies. A – D are CS18. E – H are CS19. I – L are CS20. A, E & I are sagittal views. B, F & J are coronal views. C, G & K are cephalic dorsal views. D, H & L are caudal dorsal views. Scale bar represents 1.5 mm. n = 1.

interdigital tissue, gave the forelimb the appearance of a wing (Fig. 2, E & F). The plagiopatagium appeared to have expanded from the proximal edge of digit 5 to the proximal edge of digit 1 of the hind limb (Fig. 2, E). There was a dermal outgrowth in the region of the uropatagium (tissue that spans ankle to tail) (open, white arrow in Fig. 2, H). The hind limbs appeared similar in shape and were symmetric in overall shape unlike the forelimb, which began to show unique morphologies. When comparing the length of the hind limbs to the CS15 embryo there was a change in size. At CS15 the distal tip of the hind limbs even with the distal tip of the tail. At this stage the distal tip of the tail was across from the ankles of the hind limbs. There was also external evidence of digit condensations in the hind limbs (Fig. 2, E & F).

The CS17 embryo, collected in 2007, sample 030 (Fig. 2, I – L) exhibited a wrinkling texture in several areas of the epidermis. This was not observed in other stages examined. The pinnae had grown larger when compared to the CS16 embryo and began to curve towards the eyes (Fig. 2, I & J). The vibrissae protruded from the face more when compared to the CS16 embryo. The large size of the forelimbs in proportion to the body resulted in the forelimbs being tucked under the chin and hind limbs of the embryo (Fig. 2, I & J). Measurements of the growth at this stage showed the body widening by 0.447 mm when compared to CS16. The length of the distal forelimb had increased 1.787 mm from CS16. The propatagium exhibited a thickening along the distal edge and had increased in overall surface size. The distal edge of the dactylopatagium had receded in the interdigital areas. Digits 1 – 4 were hidden behind the chin and hind limbs (Fig. 2, I & J). The plagiopatagium had increased in surface area and was protruding away from the trunk of the embryo. The uropatagium had increased in surface area (Fig. 2, L). The

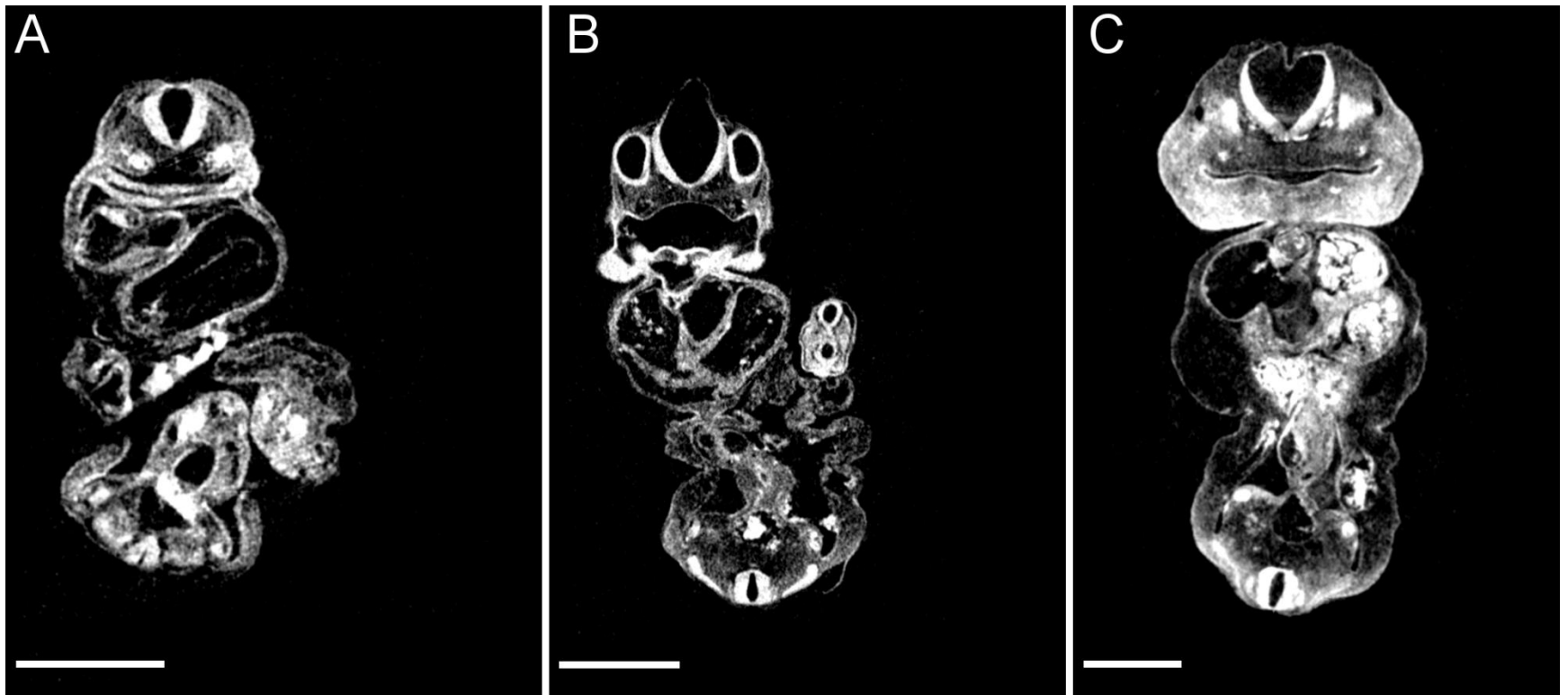


Figure 4: Internal renderings of *Carollia perspicillata* embryos from micro-computed tomography, showing internal morphologies. Shown is a coronal slice, near midline, to view internal morphologies. A is CS11. B is CS12. C is CS13. Scale bar represents 0.5 mm. n = 1.

hind limbs appeared to be longer in proportion to the embryo and there was more narrowing of the distal tips of the digits (Fig. 2, I & J). The tail was protruding minimally from the uropatagium when compared to the CS16 embryo (Fig. 2, I & J).

The CS18 embryo, collected in 2005, sample 009 (Fig. 3, A – D) showed dermal thickening around all areas of the developing eyes (Fig. 3, A & B). The pinnae had begun to curl around itself (Fig. 3, A & B). The nostrils had a more mature appearance when compared to the CS17 embryo (Fig 3, A & B). The forelimbs had increased in size and were no longer tucked below the chin. They were still tucked behind the hind limbs (Fig. 3, A & B). Digit condensations were longer and the forelimb was large enough to hide the nose and jaw (Fig. 3, A & B). There appeared to be distinct differences in the digits. Digit 1 was protruding from the dactylopatagium, which showed some regression between digit 1 and 2 leaving digit 1 appearing as an individual (free) digit. The other patagia were increased in size. Digit 2 appeared much shorter than digits 3-5 (Fig. 3, A & B). The interdigital tissue of the hind limb had regressed leaving the 5 digits free. The distal tips of the digits were free after the interdigital tissue had regressed, and all 5 were similar to each other (Fig. 3, B). The tail no longer protruded from the uropatagium (Fig. 3, D). When comparing this stage to the previous CS17 embryo there was external evidence of tendons of both the forelimbs and hind limbs.

The CS19 embryo, collected in 2005, sample 112 (Fig. 3, E – F) showed further development of the pinnae when compared to the CS18 embryo. The pinnae had curled around towards the inner ear slightly more than the previous stage (Fig. 3, E & F). The forelimbs were larger. Digit identities were more pronounced. Digit 1 was longer, and

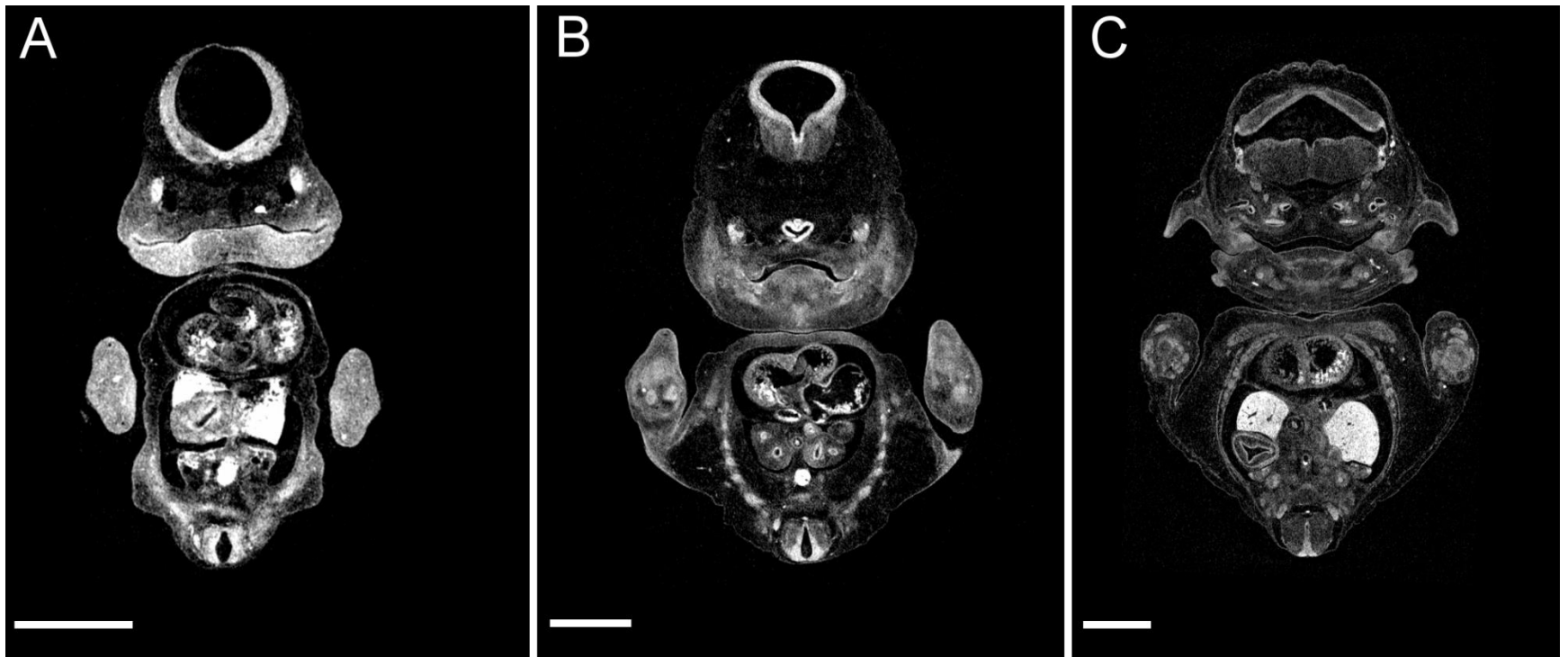


Figure 5: Internal renderings of *Carollia perspicillata* embryos from micro-computed tomography, showing internal morphologies. Shown is a coronal slice, near midline, to view internal morphologies. A is CS14. B is CS15. C is CS16. Scale bar represents 1 mm. n = 1.

the dactylopatagium was further regressed, leaving the digit free. Digit 2 had increased in size, but was still shorter than digits 3 – 5 (Fig. 3 (E, F & G). The patagia had increased in surface areas when compared to the CS18 embryo and there was a thickening to the distal edges (Fig. 3, E – H). The interdigital tissue of the hind limbs appeared to be fully regressed, leaving individual digits free (Fig. 3, E, F & H). As seen in the CS18 embryo, all 5 digits were highly similar to the each other. The tail was fully encompassed in the uropatagium (Fig. 3, H). Tendons were visible and more pronounced than they were in the CS18 embryo.

The CS20 embryo, collected in 2012, sample 149 (Fig. 3, I – L) showed an increase in forelimb size. At CS19 the length of the distal forelimb from wrist to the distal tip of digit 3 was 2.988 mm and at CS20 the length was 4.452 mm. The forelimbs masked the face making observations of further external craniofacial development not possible (Fig. 3, I & J). The ears were left unexposed and the pinnae had increased in size (Fig. 3 I, J & K). The pinnae still curled slightly towards the internal ear, but extended size now gave the appearance of more mature ears. The size of the forelimbs in this stage compared to that of the previous stage was striking. Each of the five digits appeared to have lengthened distally as well thickened (anterior to posterior). Digit 1 also showed evidence of a nail. The patagia had further increased in surface area when compared to the CS19 embryo (Fig. 3, I, J & L). The propatagium was nearly touching the bottom of the ear. The dactylopatagium was smoother along the distal edges of the wing. The plagiopatagium had increased in surface area to the point that it was now folded towards the body and could not be fully visualized externally. The uropatagium was also masked from external observations due to the growth of the hind limbs

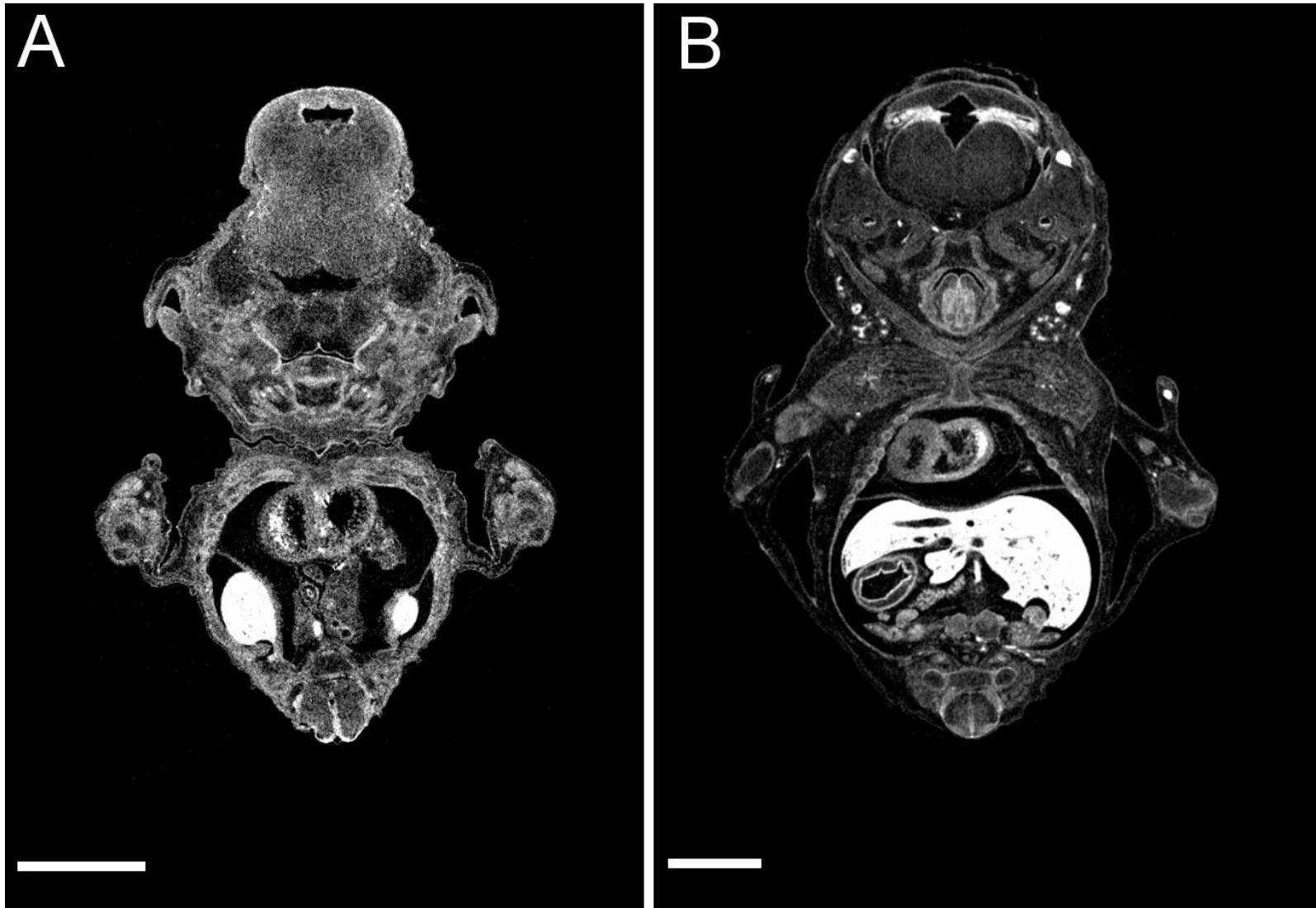


Figure 6: Internal renderings of *Carollia perspicillata* embryos from micro-computed tomography, showing internal morphologies. Shown is a coronal slice, near midline, to view internal morphologies. A is CS17. B is CS18. Scale bar represents 1.5 mm. n = 1.

(Fig 3, J & L). Consistent with the previous stages (CS18 & 19) each digit of the hind limb was similar in appearances, and each displayed a developing nail at the distal tip. The tendons of the forelimbs and hind limbs were visible and were more developed than the CS19 embryo. Hair follicles were also present at this stage. This gave the embryo a speckled appearance on the dermal surface.

Internal micro-CT

Using μ CT to examine *C. perspicillata* embryos resulted in highly detailed internal morphological data along with the external morphologies previously described. We used these internal morphologies and focus on a single internal coronal slice of each embryo, from CS11 – 20. The coronal slice was taken near the midline of the developing embryos. We briefly describe a few internal morphological features to demonstrate the future potential of the data obtained. We examined these slices and looked for variations in contrast that may indicate the presence of differing tissue densities and types.

The CS11, 12, & 13 embryos (Fig. 4, A, B & C) were visualized first. The external descriptions of these stages showed a twist to the left in the caudal portion of the embryo as well as somite pairs numbering from 22 – 32. Present throughout these stages was evidence of the neural tube (precursor to the central nervous system). The neural tube could be seen in both cephalic and caudal regions. These stages showed a region in the center of the neural tube with no contrast (black), showing the neural tube lumen (hollow interior). Areas near the cephalic end of the embryos at these stages were highly similar in contrast, which may have indicated a single tissue type or unvarying density. Towards the caudal end of the embryos at these stages there were some areas of differing shades of grey and white, which may have indicated areas of varying tissue densities or types. The area where the heart was beginning to develop through these stages showed increasing complexity in contrast differences, and by CS13 there appeared to be a hollow chamber surrounded by a high contrasting tissue.

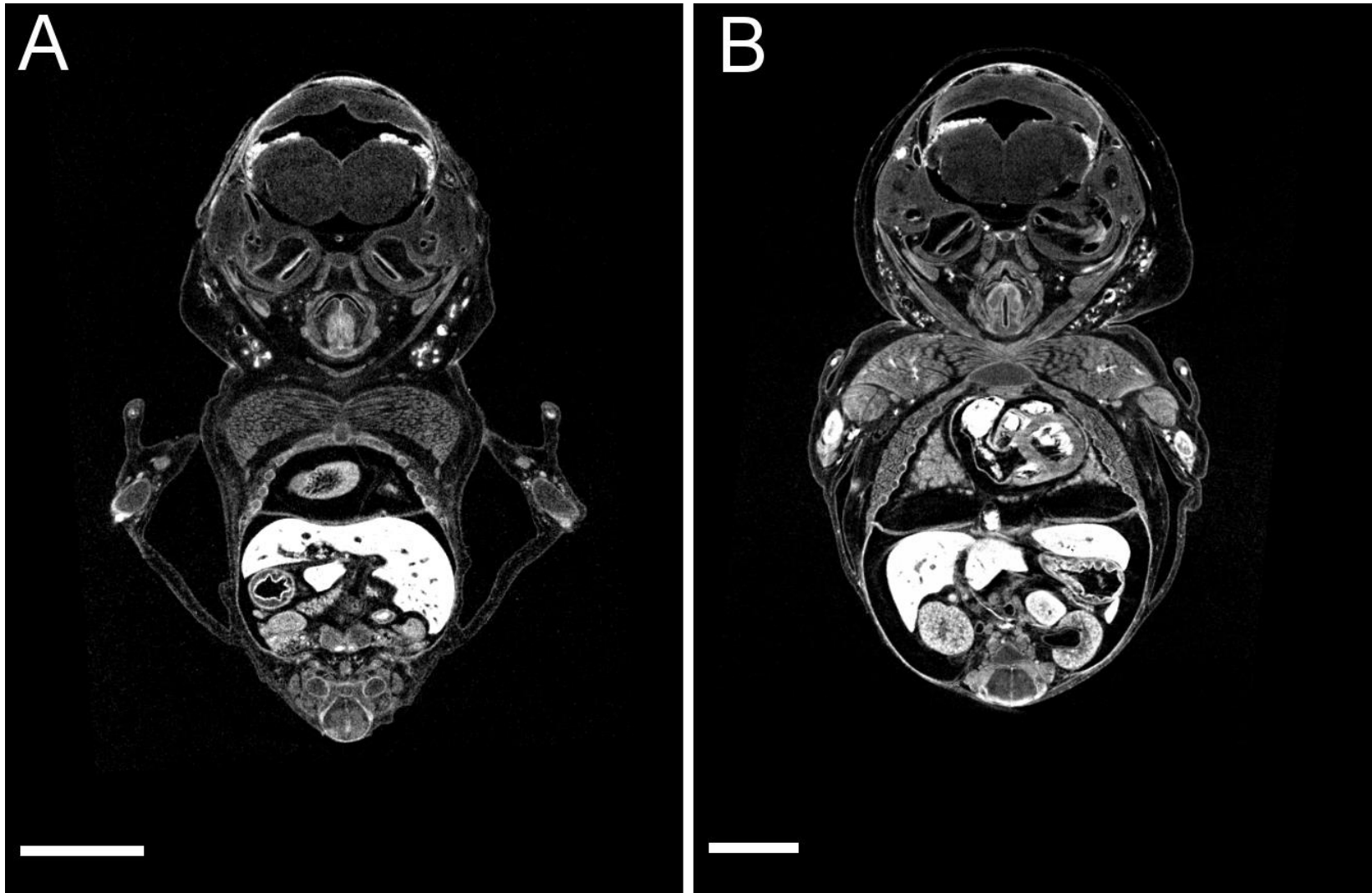


Figure 7: Internal renderings of *Carollia perspicillata* embryos from micro-computed tomography, showing internal morphologies. Shown is a coronal slice, near midline, to view internal morphologies. A is CS19. B is CS20. Scale bar represents 2 mm. n = 1.

Next we visualized CS14, 15 & 16 (Fig. 5, A, B & C). The external morphologies showed the increasing size and complexity of the forelimbs, the completion of somitogenesis, changes in pharyngeal arches and development of more mature facial features. Internally, throughout these stages, the caudal region of the neural tube changed from having a lumen at CS14 to being closed at CS16. This change in the caudal neural tube through these stages was accompanied by an increase in varying contrast differences in the cephalic region of the embryos. Throughout these stages there was also increasing contrast differences seen in the facial region of the embryos, indicating increased complexities of the tissues that were present. These stages also included the forelimb in the coronal slice. The contrast increasingly varied in the forelimb region throughout the stages. From CS14 there was little contrast in the forelimb region, with an increase in complexity by CS15 and the CS16 embryo showed distinct contrast differences between thin tissues and denser, mineralized tissues. The thoracic area showed an increase in contrast complexities in the developing heart, resulting in two of the four chambers being visible in CS16 embryo. At CS15 we see high contrast in areas of rib development, in the CS16 embryo there was evidence of the diaphragm (separates thoracic and abdominal cavity). Throughout these stages there was an increasing amount of contrast variation in the abdominal cavity where organs were developing. In CS16 the bright contrasting area in the abdominal cavity is the developing liver.

Figure 6 shows the coronal slice of both CS17 & 18 (A & B respectively). These stages were previously described externally highlighting the remarkable changes in forelimb size and increasingly maturing external features of the face and patagia. Internally the head showed increasing contrast complexities in the areas of the developing

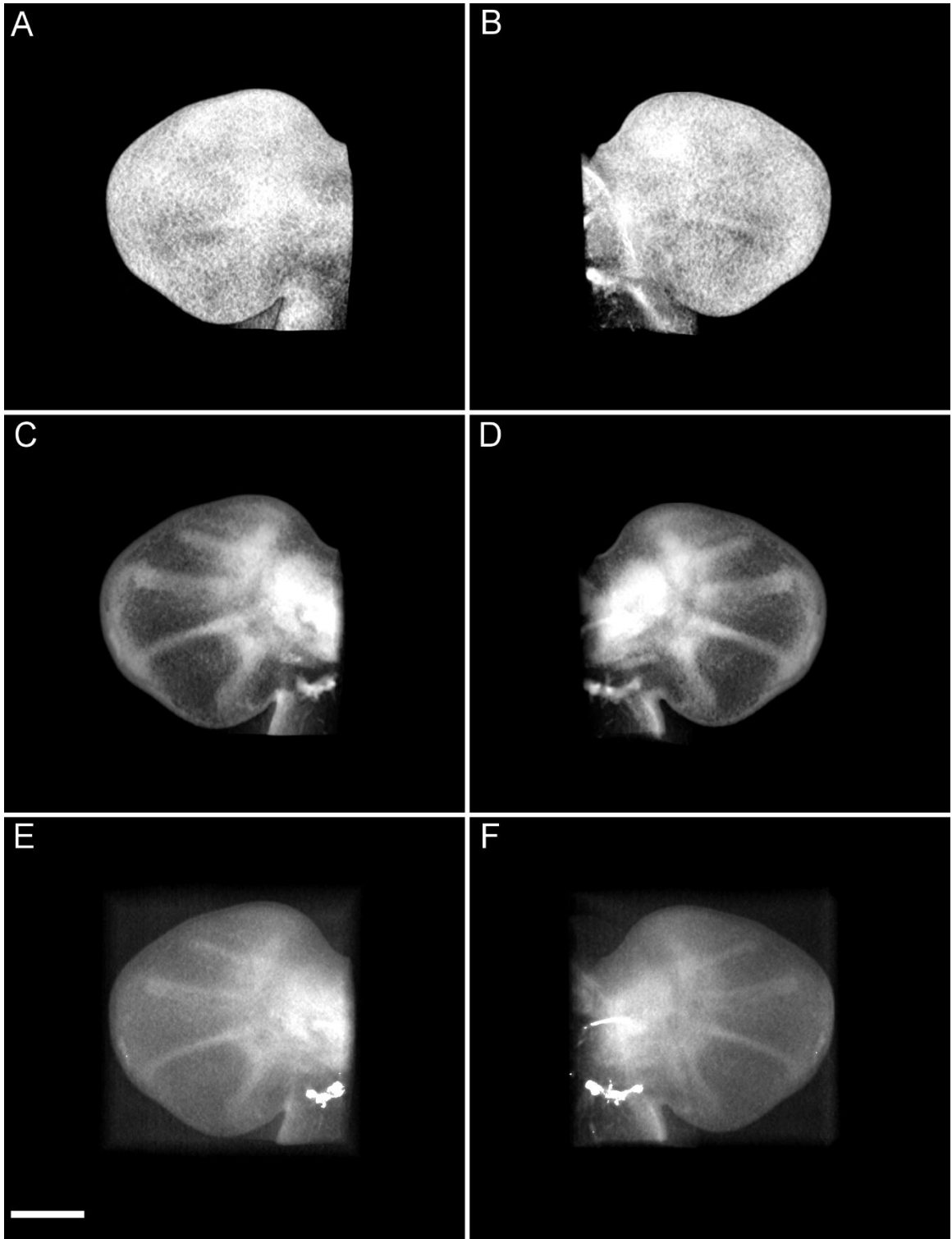


Figure 8: Surface and internal renderings of *Carollia perspicillata* forelimbs from micro-computed tomography, showing developing forelimb morphologies. Dorsal (left column) and ventral (right column) views of the left CS15 forelimb, sectioned away from whole embryo. A & B show surface view. C & D show internal view. E & F show varied contrasts of internal view. Scale bar represents 0.5 mm. n = 1.

brain and face. Anterior to the thoracic chamber in both CS17 & 18 there was evidence of muscles developing. The developing ribs showed higher contrast at the outer edges, with less contrast inside. The heart resembled what was seen in the CS16 embryo, with individual chambers with no contrast being surrounded by contrasting tissues. Increasing complexity in contrast in the abdominal cavity was observed in these stages.

CS19 & 20 embryos were examined next (Figure 7, A & B). The external morphological examination described these stages displaying increased tendon development in the forelimbs and hind limbs, increasing sizes of fore and hind limbs and the first appearance of hair follicles. Internally these stages were consistent with CS17 & 18, with contrast complexities continuing to increase throughout the body. These stages showed increased contrasting complexity anterior to the thoracic chamber where muscles were developing. The CS20 embryo showed contrasting areas where the lungs were developing in the thoracic cavity. The abdominal cavity showed several variations in contrast where many organs were beginning to show a more mature form.

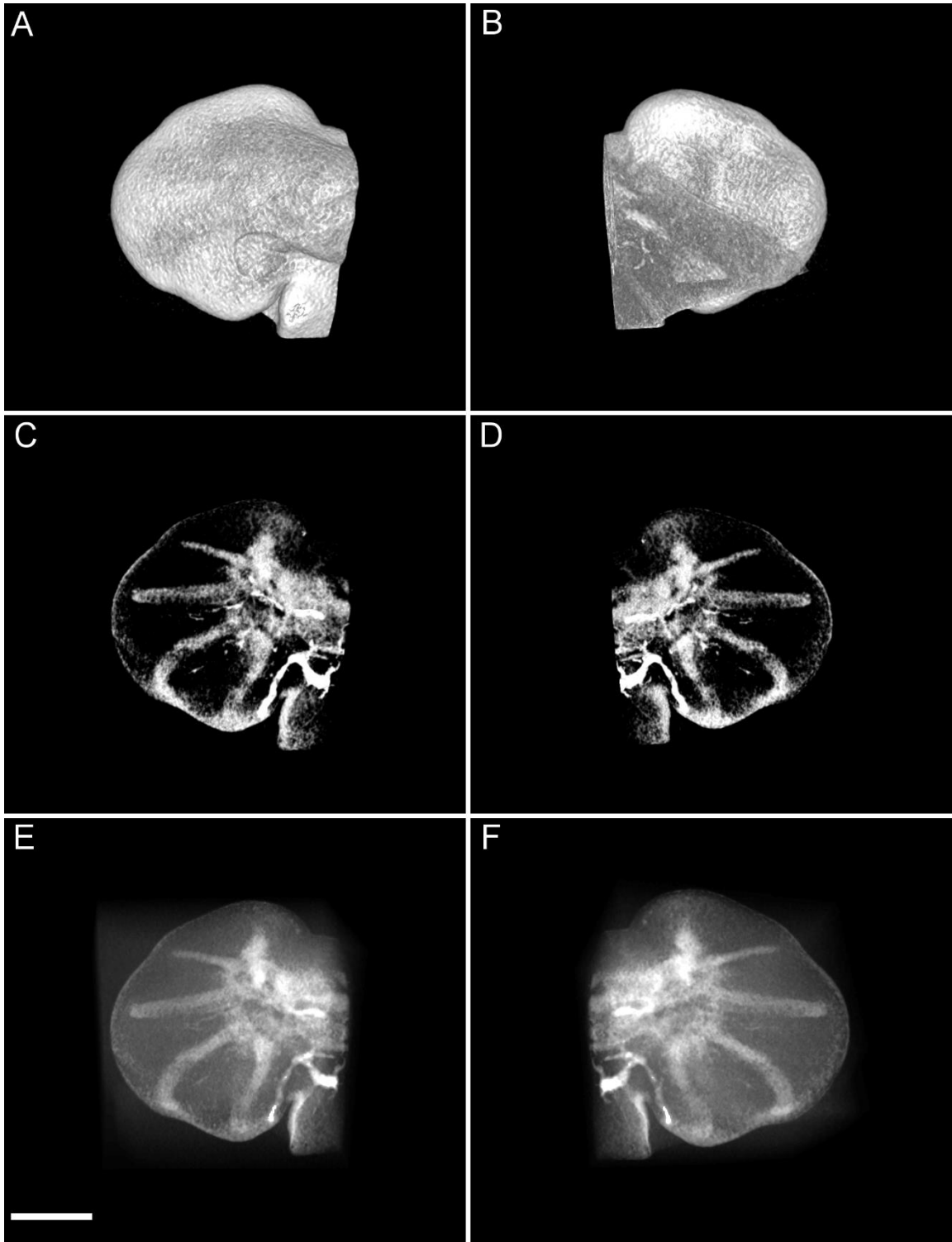


Figure 9: Surface and internal renderings of *Carollia perspicillata* forelimbs from micro-computed tomography, showing developing forelimb morphologies. Dorsal (left column) and ventral (right column) views of the left CS16 forelimb, sectioned away from whole embryo. A & B show surface view. C & D show internal view. E & F show varied contrasts of internal view. Scale bar represents 0.5 mm. n = 1.

Forelimb micro-CT

Now that we have demonstrated the use of μ CT in describing both external and internal morphologies of the developing *C. perspicillata* embryo through 10 stages of development (CS11 – 20) we next focused on the development of the bats highly adaptive forelimb. We rely on the differences in contrast in the forelimb tissues to determine stages of *C. perspicillata* embryos to use in the upcoming whole-mount *in situ* hybridization experiments. Because μ CT relies on differences in tissue densities, we focus on CS15 - 20. Earlier stages of development (CS11 – 14) showed no contrast differences in forelimb tissue making images from these stages a single contrast. Later stages (CS15 – 20) had enough contrast variation to make observations on initial digit condensations, cartilage development, joint development, some muscular development, vascularization and differences in digit identities.

CS15 forelimbs (Fig. 8, A – F) showed the first significant signs of cellular condensation. At CS15, the condensations could be seen in the areas where digits 1 – 5 are known to be located. Condensations could also be seen in areas where wrist elements are located. The areas of condensation were similar in contrast to that of the surrounding soft tissue elements. At this stage there were signs of vascularization (Fig. 8, C – F). The area posterior to the condensations in the hand plate (bright white areas in Fig 8, E & F) suggests the presence of vascularization of the forelimb. There were differences in digit length, but the tissue that was present was homogenous. The lack of varying contrast in the digit condensations indicated that it was too early to see other digit identity elements (individual phalanges and joints).

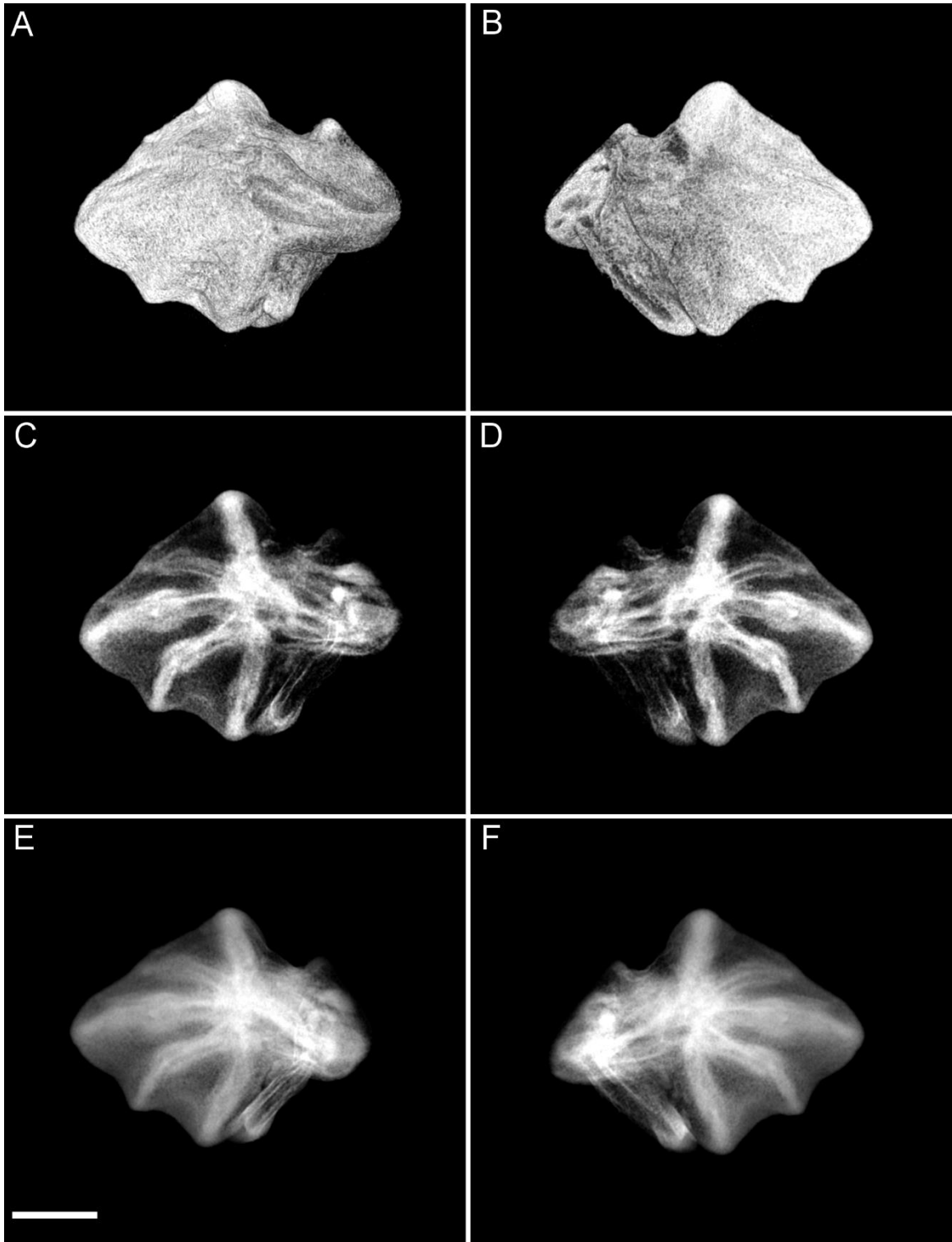


Figure 10: Surface and internal renderings of *Carollia perspicillata* forelimbs from micro-computed tomography, showing developing forelimb morphologies. Dorsal (left column) and ventral (right column) views of the left CS17 forelimb, sectioned away from whole embryo. A & B show surface view. C & D show internal view. E & F show varied contrasts of internal view. Scale bar indicates 1 mm. n = 1.

CS16 forelimbs (Fig. 9, A – F) showed more structural detail in the areas of condensation when compared to the CS15 forelimb. The contrasting areas varied more than the areas of soft tissue elements surrounding them. The area of vascularization posterior to the hand plate had increased in length towards the distal end of digit 5. Overall digit lengths were still distinguishable however, the structural details of other elements were still not present.

CS17 forelimbs (Fig. 10, A – F) showed an overall change in shape, no longer resembling a paddle. There were now several variations in contrast visible. Digit condensations varied from the soft tissue more. The digit condensations were more structurally detailed than the CS16 forelimb and began to look like the mature form. There were clear indications of shape change in digits 2 – 4 in the area of the first joint. Digit lengths were still distinguished, and at CS17 there was evidence of varying identities. Digit 1 appeared to have a single phalanx with one joint on the distal end of the metacarpal. Digit 2 appeared to have 1 shortened phalanx with 1 joint at the distal metacarpal edge. Digit 3 had 2 distinguishable phalanges, both large, with 2 joints at the distal metacarpal edge and the phalanx distal to the metacarpal. Digit 4 had 2 phalanges with 2 joints, and a distinct curve at the distal end, towards the caudal end of the embryo. Digit 5 appeared to have 1 phalanx with 1 joint at the distal metacarpal edge.

CS18 forelimbs (Fig. 11, A – F) showed a loss of interdigital mesenchyme between digits 1 and 2, resulting in digit 1 being freed. Areas of contrast had become more structurally detailed than the CS17 forelimb which allowed for visualization of

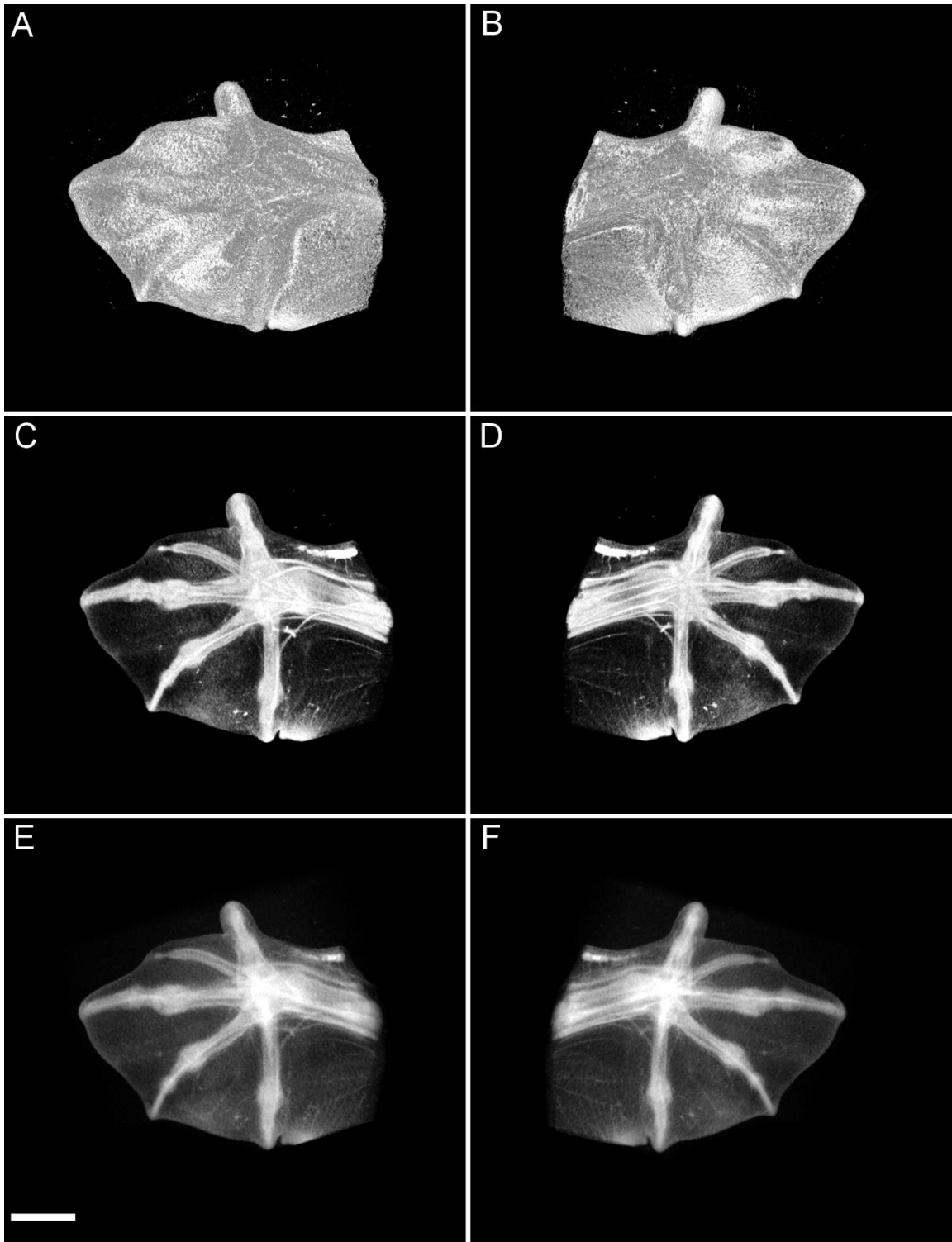


Figure 11: Surface and internal renderings of *Carollia perspicillata* forelimbs from micro-computed tomography, showing developing forelimb morphologies. Dorsal (left column) and ventral (right column) views of the left CS18 forelimb, sectioned away from whole embryo. A & B show surface view. C & D show internal view. E & F show varied contrasts of internal view. Scale bar represents 1 mm. n = 1.

several digit elements in the CS18 forelimb. The joint distal to the metacarpal of digit 1 was more detailed as was the phalanx. Digit 2 was also more detailed, showing a very reduced phalanx and a single joint distal to the metacarpal. Digit 3 had two joints as well as 2 phalanges. Digit 4 had two joints and 2 phalanges distal to the metacarpal. Digit 5 appeared to have a single joint and phalanx. The increasing detail in CS18 allowed for visualization of tendons that come down the forelimb and attach towards the distal ends of each digit. Vascularization of the distal elements can also be determined at CS18. Vascularization could also be visualized in the dactylopatagium.

CS19 forelimbs (Fig. 12, A – F) showed the first external evidence of vessels and tendons being present. There was evidence of a second joint on digit 1. Digit 3 had an area that appeared to be a third joint near the distal end. Tendons were still visualized, but the contrast was close to that of the digits making them difficult to visualize individually. Vascularization had increased in the dactylopatagium. Digits 1, 4 & 5 all had 2 joints and 2 phalanges. The distal tip of digit 2 appeared highly reduced when compared to the distal phalanges of the other digits. Digit 3 was showed 3 joints and 3 phalanges.

CS20 forelimbs (Fig. 13, A – F) showed the most structural detail in the tissues present in the forelimb. Tendons could be identified individually, running along the digits towards the distal end. Vessels were individually identifiable in the distal forelimb, along digits and throughout the dactylopatagium. Digits 1, 4 & 5 had 2 joints and 2 phalanges, however digit 1 had not lengthened much when compared to digits 4 and 5. Digit 2 had one joint, 1 phalanx and it remained highly reduced in size. Digit 3 had three

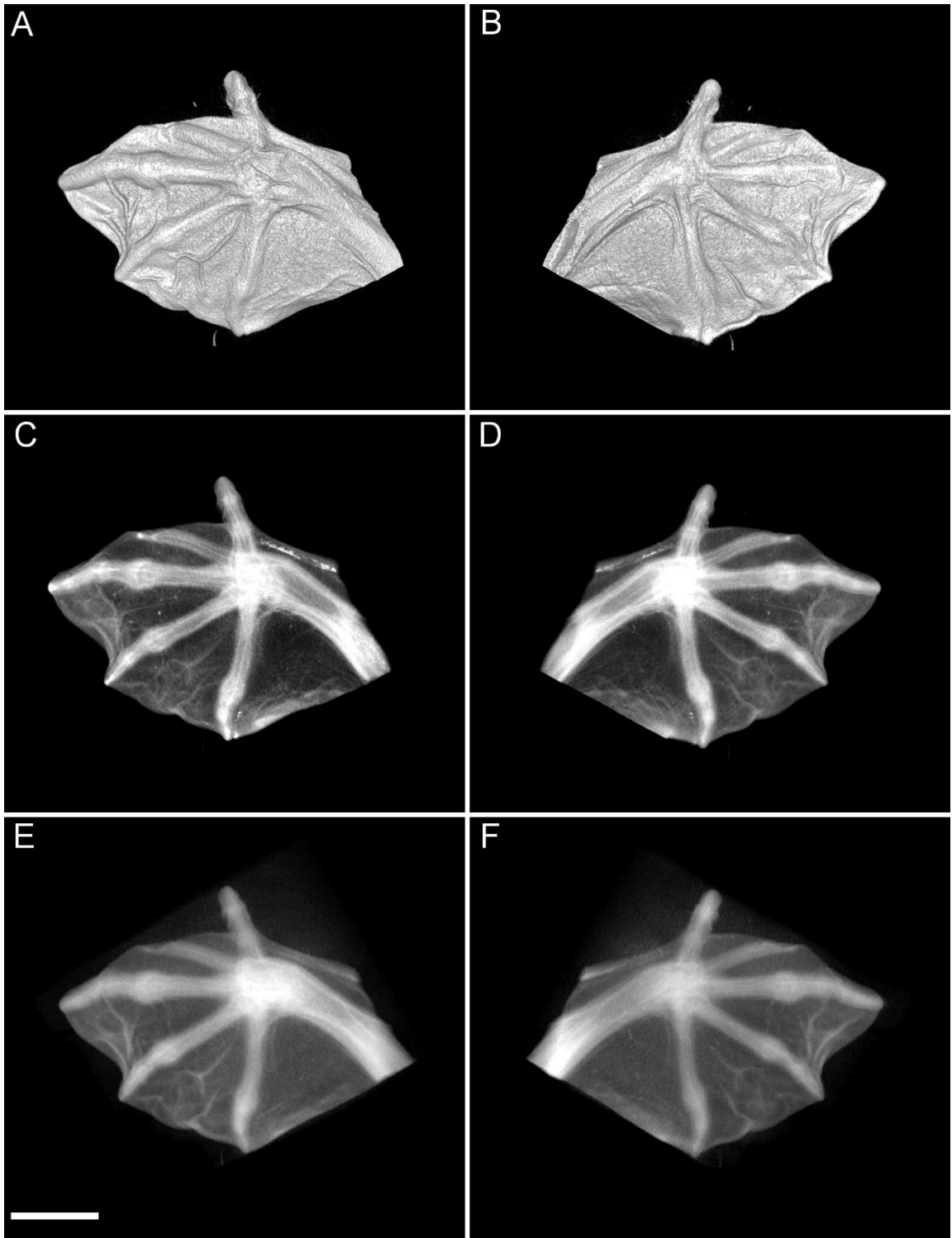


Figure 12: Surface and internal renderings of *Carollia perspicillata* forelimbs from micro-computed tomography, showing developing forelimb morphologies. Dorsal (left column) and ventral (right column) views of the left CS19 forelimb, sectioned away from whole embryo. A & B show surface view. C & D show internal view. E & F show varied contrasts of internal view. Scale bar represents 1.5 mm. n = 1.

joints and 3 phalanges. At this point the developing forelimb was more similar to the mature form, but final digit identities had still not been achieved.

Measurements of each digit condensation as they progressed through development (Fig. 14) shows the rapid nature of growth in the forelimb in CS15 – 20. Digit 1 was not present in CS15, but at CS16 it measured 0.205 mm and by CS 20 it was 1.828 mm. Digit 2 started at 0.359 mm in CS15 and was at 2.281 mm by CS20. Digit 3 was 0.55 mm at CS15 and grew to 4.977 mm by CS20. Digit 4 was at 0.521 mm at CS 20 and grew to 3.939 mm by CS20. Digit 5 was at 0.422 mm at CS15 and grew to 3.976 mm by CS20.

Throughout the 24 days in development the digits had changed remarkably in size. Digit 1 extended a total of 1.828 mm. Digit 2 extended 1.922 mm throughout the 24 days. Digit three, showing the largest total change in length, extended 4.427 mm. Digit 4 extended 3.418 mm total. Digit 5 extended a total of 3.556 mm in 24 days.

Digit 1 grew 8.9 times its initial measured size in 20 days. Digit 2 grew 6.4 times its original size in 24 days. Digit 3 grew 9 times its original size in 24 days. Digit 4 grew 7.6 times its original size in 24 days. Digit 5, although not the longest digit at this stage, showed the highest growth rate. It grew 9.5 times its original size in 24 days.

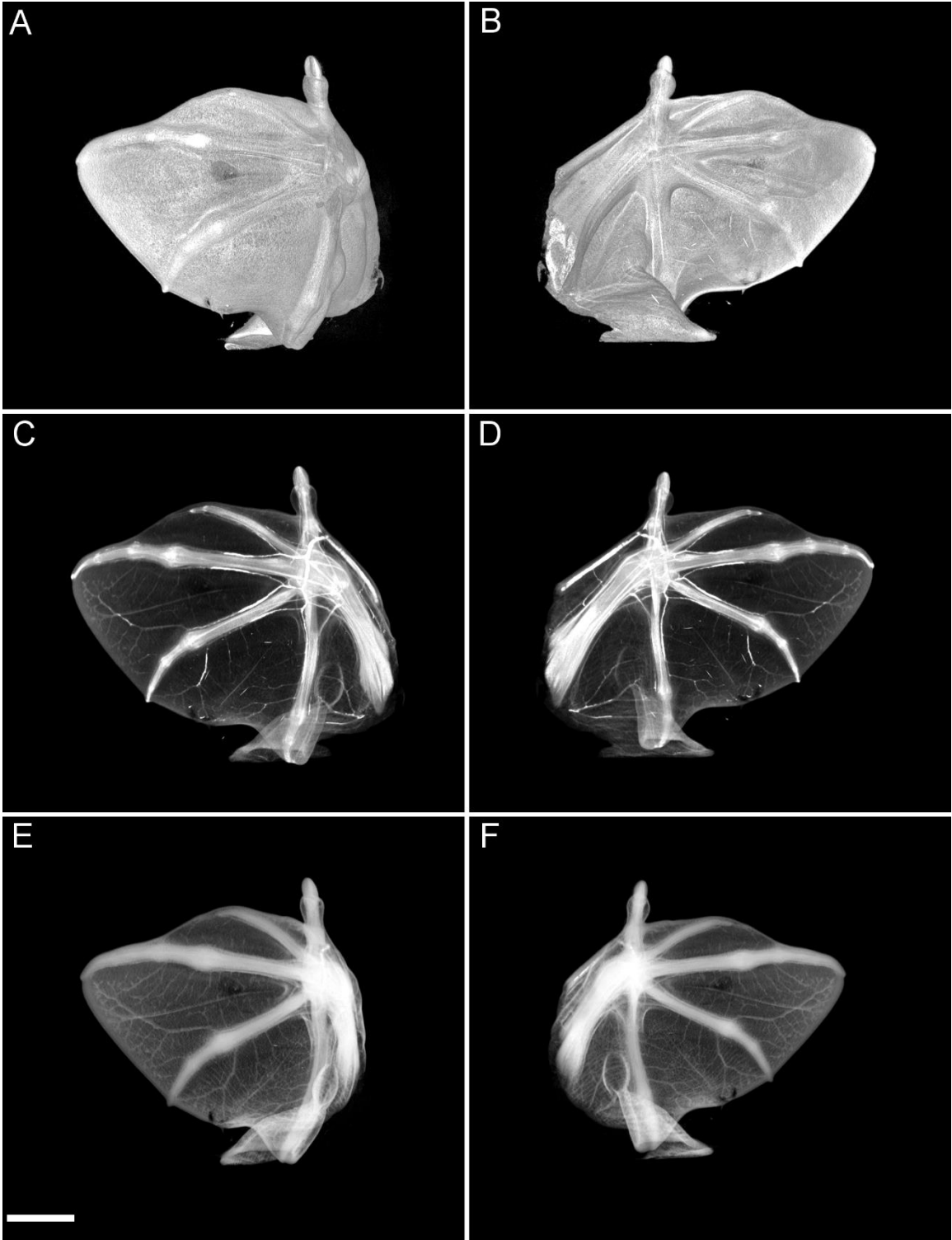


Figure 13: Surface and internal renderings of *Carollia perspicillata* forelimbs from micro-computed tomography, showing developing forelimb morphologies. Dorsal (left column) and ventral (right column) views of the left CS20 forelimb, sectioned away from whole embryo. A & B show surface view. C & D show internal view. E & F show varied contrasts of internal view. Scale bar represents 2 mm. n = 1.

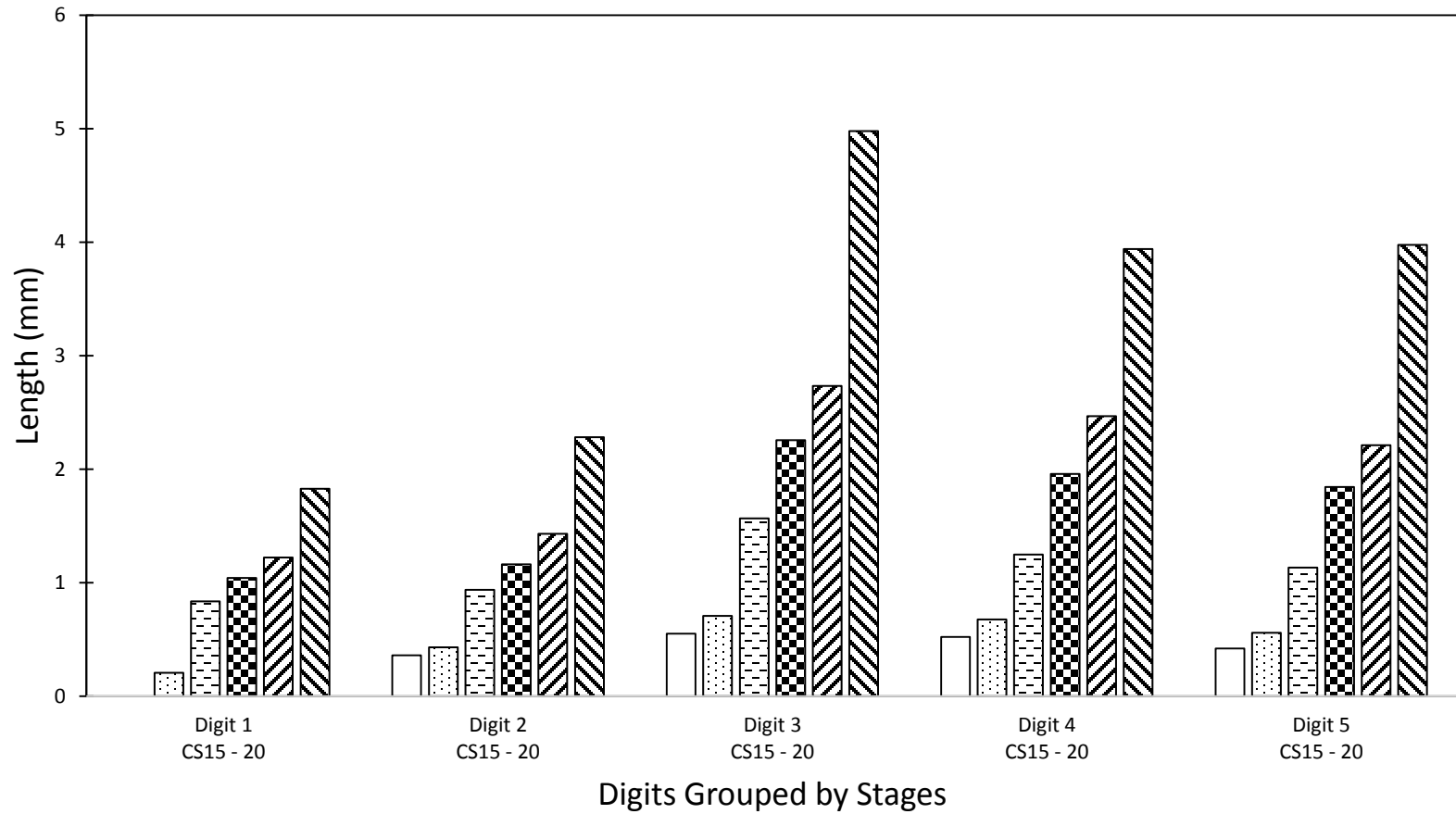


Figure 14: Digit lengths (mm) grouped in stages of development. Open bar is CS15. Spotted bar is CS16. Horizontal dashed bar is CS17. Checkered bar is CS18. Right-angled dashed bar is CS19. Left-angled dashed bar is CS20. n = 1.

Table 1: List of embryos used in micro-CT scans. 3 embryos from each stage were scanned. The highest quality scan of each stage was then chosen for the descriptions.

Embryos Used for μCT		
Stage	Year Collected	Specimen Number
CS11	2007	019
	2014	133
	2014	193
CS12	2010	165
	2010	166
	2010	174
CS13	2014	173
	2014	178
	2014	188
CS14	2007	047
	2007	053
	2007	070
CS15	2011	104
	2011	199
	2011	176
CS16	2001	179
	2007	029
	2007	040
CS17	2007	169
	2007	030
	2000	057
CS18	2005	009
	2005	046
	2005	051
CS19	2000	091
	2005	112
	2005	144
CS20	2012	106
	2012	149
	2012	161

Whole-mount *in situ* Hybridization:

After examining the μ CT data it was determined that stages CS15 – 17 were appropriate candidates in the WISH portion of the study. Using primers described in Chapter II (page 14), resulted in a 715 base pair PCR product (Fig. 15). This was sequenced and verified to be identical to the composite *C. perspicillata* RNA sequence from RNAseq data, and over 90% identical to known *Cyp26b1* sequences from other bats and mammals (BLAST RID - SAWWS17701R). The RNA probe (riboprobe) was synthesized using the sequenced DNA that was ligated into the vector plasmid. The riboprobe was located near the 3' end of the *Cyp26b1* gene.

```
5'... ATGCTCTTTGAGGGCTTGGAGCTGGTGTCTGGCGCTGGCCACCCTCGCCGCGTGCCTGGTGTCCGGTGACGCTGCT  
GCTGGCCGTGTCTGCAGCAGCTGTGGCAGCTGCGCTGGGCTGCCACTCGCGACAAGAGCTGCAAGCTGCCCATCCCC  
AAGGGCTCCATGGGCTTCCCCTCATCGGAGAGACCGGCCACTGGCTGCTACAGGGTTCTGGCTTCCAGTCGTAC  
GGAGGGAGAAGTACGGCAACGTGTTCAAGACGCACTTGCTGGGGCGGCCGCTGATCCGCGTGACAGGCGCGGAGA  
ACGTCCGCAAAATCCTCATGGGTGAGCACCCTCGTGAGCACAGAATGGCCGCGCAGCACGCGCATGCTGCTGGG  
CCCGAACACAGTGGCCAACCTCATCGGCGACATCCACCGCAACAAGCGCAAGATATTCTCCAAGATCTTCAGCCAC  
GAGGCTCTGGAGAGCTACCTGCCAAGATCCAGCTGGTATCCAGGACACGCTGCGTGGAGCAGCCGCCCTG  
AGGCCATCAACGTGTATCAGGAAGCACAGAAGCTCACCTTCCGCATGGCCATCCGAGTACTCCTGGGCTTACGCAT  
CCCTGAAGAAGACCTCGGGCACCTCTTCGAGGTCTACCAGCAGTTTGTGGAGAATGTGTTCTCCCTGCCTGTCGACT  
TGCCCTTTAGTGGCTACCGGCGGGGCATTCAGGCACGACAGACCCTGCAGAAGGGCCTGGAAAAGGCCATCCGGG  
AGAACTGCAGTGCACGCAGGGCAAGGACTACTCGGACGCGCTGGACATCCTCATTGAGAGCAGCAAGGAGCACG  
GGAAGGAGATGACCATGCAGGAGCTGAAGGACGGGACCCCTGGAGCTGATCTTTGCCGCTATGCCACCAGGCCA  
GCGCCAGCACCTCACTCATCATGCAGCTGCTGAAGCACCCGGCTGTGCTGGAGAAGCTGCGGGAGGAGCTGCGGGC  
CCACGGCATCCTGCACAGCGGCGGCTGCCCTGCGAGGGGACGCTGCGTCTCAGCACCCCTCGGCGCCTGCACTAC  
CTGGACTGCGTCATCAAGGAGGTGATGCGCCTTTCACGCCATTTCTGGCGGCTACCGCACCGTGTGCAGACCTT  
CGAGCTGCACGGTTTCCAGATCCCCAAAGGATGGAGTGTCATGTACAGCATCCGGGATACTACGACACAGCGCCT  
GTGTTCAAAGACGTGAACGTATTTGACCCTGACCGCTTTGGTACAGGCTCGGAGCGAAGACAAGGACGGCCGATTCC  
ATTACCTCCCTTTCGGCGGGCGGTGCCGGACCTGCCTGGGCAAGCACCTGGCCAAGCTGTTCTGAAGGTGCTGGCA  
GTGGAGCTGGCCAGCACGAGCCGCTTTGAGCTGGCCACCCGGACCTTTCCCCGAATCACGCTGGTCCCTGTCTGCA  
CCCCGTGGATGGCCTCAGTGTCAAGTCTTTGGCTGGACTCCAACCAAGAAACAAATCCTACCAGAGACAGAGGCC  
ATGCTGAGTGCCACAGTCTAACAGGGCCTGGCCACACCCCACTCAGCCCGGCCAGGCCCTGGGGTGGGAGGCCA  
ACGAAGGGTAGAAACCTGTGTGTGGGAGGGGCTGGAACCTGCGGAAGAAGAAGCAGCCCATACCTTGCCTCCCA  
TTTTTCTTCCCTGGCAAACCTACCCGAAGCCAAAAGGGTCTCCGTTCTGCTGGGGCACTGACGGGGCCCTTCTGG  
CTCCTGCTTCTCCAGTCTCTCCAGTCTCCACCAGCTTAGCTCCTGGGACAGGGCACGGCCAGGGGCTCTGCATG  
CCC ... 3'
```

Figure 15: *Carollia perspicillata* *Cyp26b1* DNA sequence. Bold text indicated the start codon and stop codon. The grey text indicates the sequence of primers, and the area in between the primers indicates the sequence of the riboprobe.

CS15 *Cyp26b1* gene expression (Fig. 16), appeared in both forelimbs and hind limbs. Expression appeared to be limited to the distal forelimb and distal hind limb regions. There were 4 clear areas of expression within the forelimb. These regions of expression appeared to be highly correlated to areas of interdigital mesenchyme, and the expression bordered areas of digit condensations. This provided evidence that the expression was contained primarily in the IDM areas.

The following stages were the primary focus of the WISH portion of the study and focused on *Cyp26b1* gene expression in CS16. The expression was examined at the primary CS16 stage as well as CS16E and CS16L. These refined stages were included to try and characterize *Cyp26b1* expression throughout the CS16 stage that was used in the RNA-seq assay.

CS16E *Cyp26b1* gene expression (Fig. 17, A), was seen in both forelimbs and hind limbs. Expression appeared to be localized to the distal forelimb and hind limb regions. The areas of expression appeared higher than they did at CS15. The expression was highest at the posterior edges of each of the 5 digit condensations. Digit 2 expression did not appear to be any higher than in other IDM regions and was measured as shorter than the areas of expression in near digit condensations of digits 3 and 4, albeit digit 2 is itself also shorter.

CS16 *Cyp26b1* gene expression (Fig. 17, B), was seen in the posterior IDM areas closely associated with the most anterior digit, except around digit 2. As seen in CS16E (Fig. 17, A), there appeared to be expression in both the posterior and anterior IDM areas surrounding digit 2. Expression can be seen posterior to all 5 developing digits in the IDM areas.



Figure 16: *Carollia perspicillata* CS15 whole-mount *in situ* hybridization expression of *Cyp26b1*. n = 1.

Expression at this stage appeared in similar areas to that seen in CS16E, however the width of areas of expression appeared wider. There did not appear to be large expression differences from one IDM area to another, although the region expression in the IDM area directly posterior to digit condensation 2 appears shorter than IDMs posterior to digits 3, 4 and 5.

CS16L *Cyp26b1* gene expression (Fig. 17, C), was found in both the forelimb and hind limb regions. Expression was limited to IDM areas in both the forelimb and hind limb. At this stage expression appeared lower than any stage previously described. Expression directly posterior to digit condensations 1 and 2 appears to be absent. Expression in IDM areas directly posterior to digit condensations 3 and 4 was still consistent with the levels seen in both CS16E and CS16.

Given RNA-seq data that showed an elevated expression of *Cyp26b1* in the IDM area directly posterior to digit 2 we were expecting a visible difference in the region of expression or clear expression differences in similar sized regions. To quantify the regions of expression we measured the length, from the proximal end to the distal end, of expression in the IDM areas posterior to digits 2 and 3. These were IDM areas shown to have the highest difference in expression in the RNA-seq data. Figure 18 shows the length comparison in each stage. In each stage, the area of expression was longer posterior to digit 3 than digit 2, suggesting that expression was increased posterior to the longer digit. In each case expression was more extensive in the IDM posterior to digit 3, in contrast to the RNAseq data.

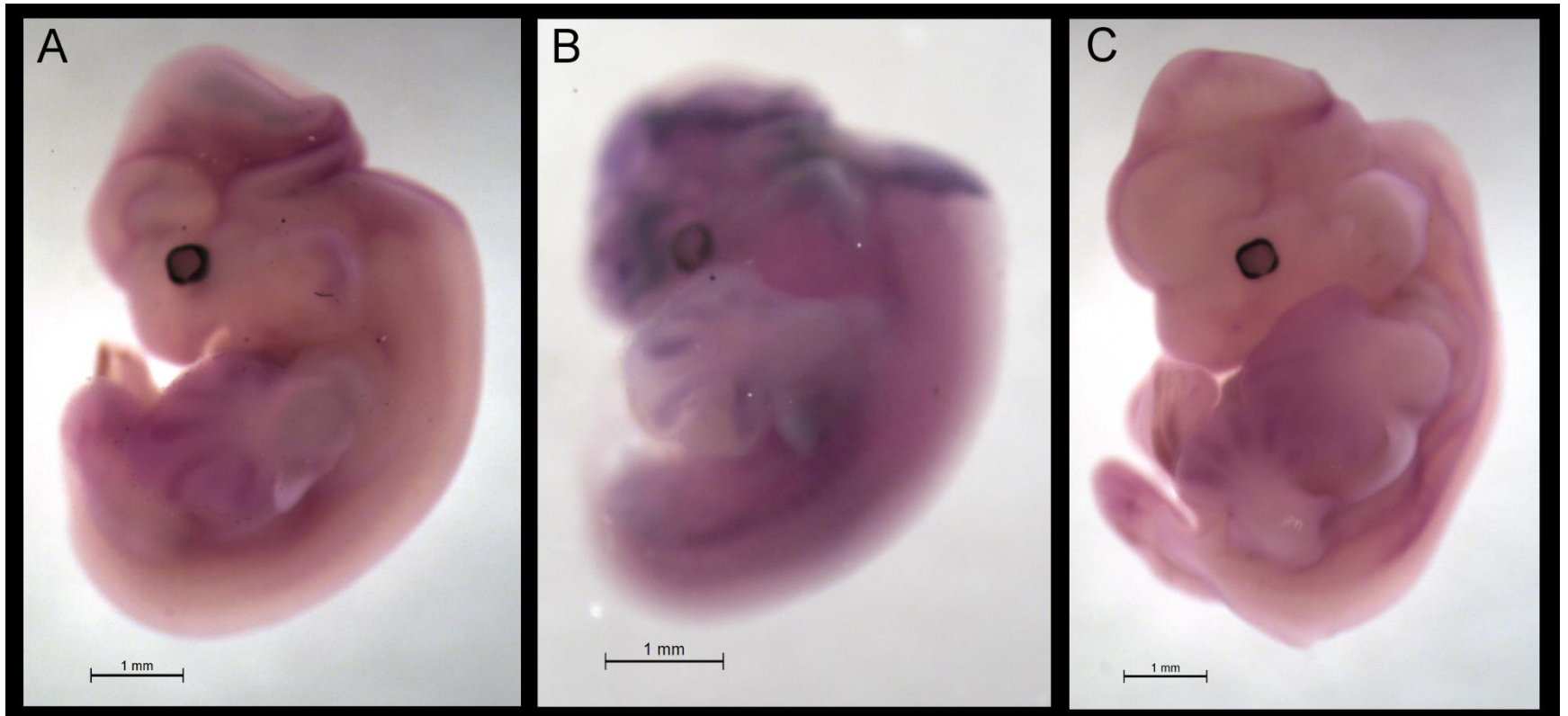


Figure 17: *Carollia perspicillata* CS16 whole-mount *in situ* hybridization expression of *Cyp26b1*. A is CS16 Early. B is CS16. C is CS16 Late. n = 1 for each stage.

Next we examined *Cyp26b1* gene expression in mouse to see if there were any unique expression patterns observed in the bat that were not displayed in mouse. Figure 19 shows *Cyp26b1* gene expression in a mouse embryo that is of a comparable stage in development as a CS16 *C. perspicillata*. Forelimb expression was confined to the distal forelimb elements, similar to what was observed in *C. perspicillata*. Expression was observed in the IDM areas primarily, also similar to what was observed in *C. perspicillata*. The concentration of expression also appeared to be similar when comparing the IDM areas posterior to digits 2 and 3. One difference observed was that the entire IDM areas showed expression where the *C. perspicillata* expression was more closely associated with the posterior edge of the digit condensations.

CS17 *Cyp26b1* gene expression (Fig. 20), was observed in forelimb and hind limb areas. Expression levels appeared reduced and limited to areas directly adjacent to digit condensations in both distal forelimb and hind limb regions. Expression at this stage was so reduced throughout the embryo we may have been observing a light trapping of the riboprobe, which is when riboprobe is trapped in hollow areas and the reaction is not showing actual gene expression.

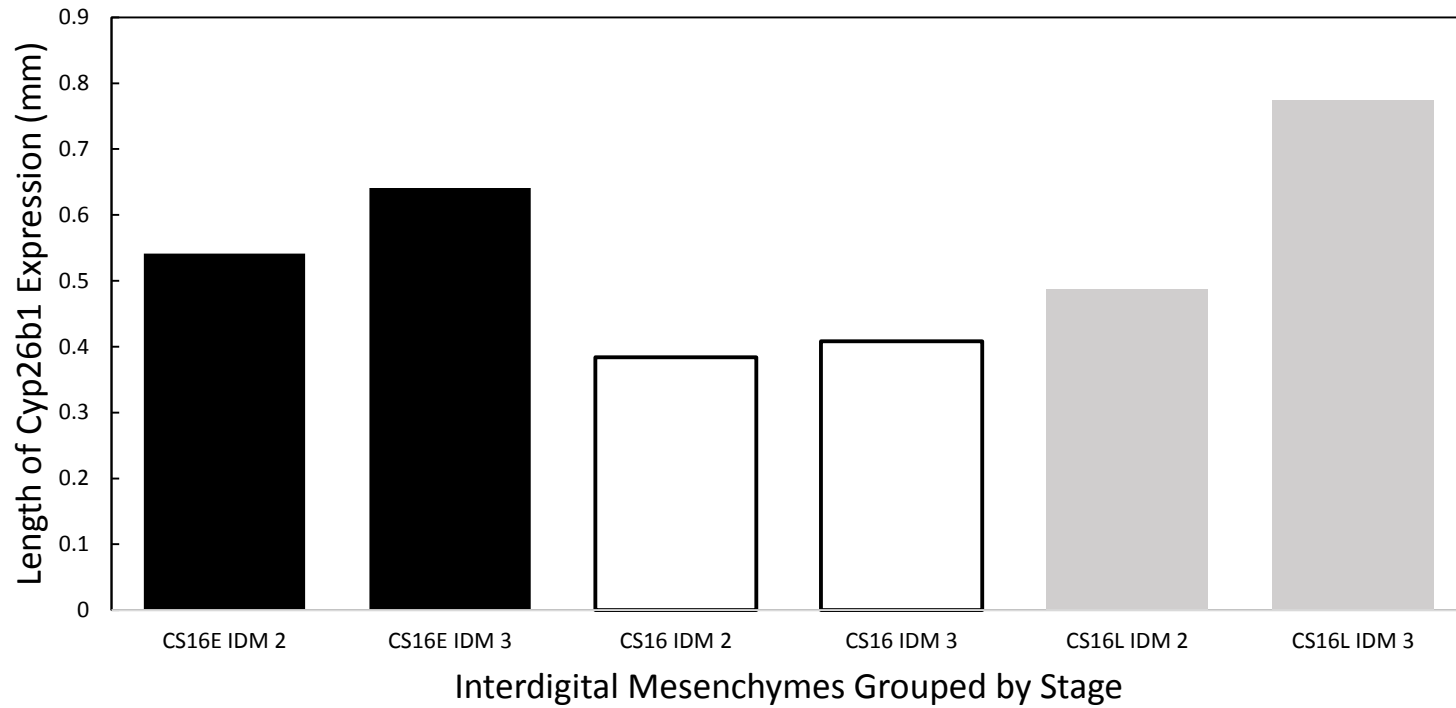


Figure 18: Proximal to distal lengths of *Cyp26b1* expression in IDM area posterior to digits 2 and 3. Black bars are CS16E. White bars are CS16. Grey bars are CS16L. n = 1.

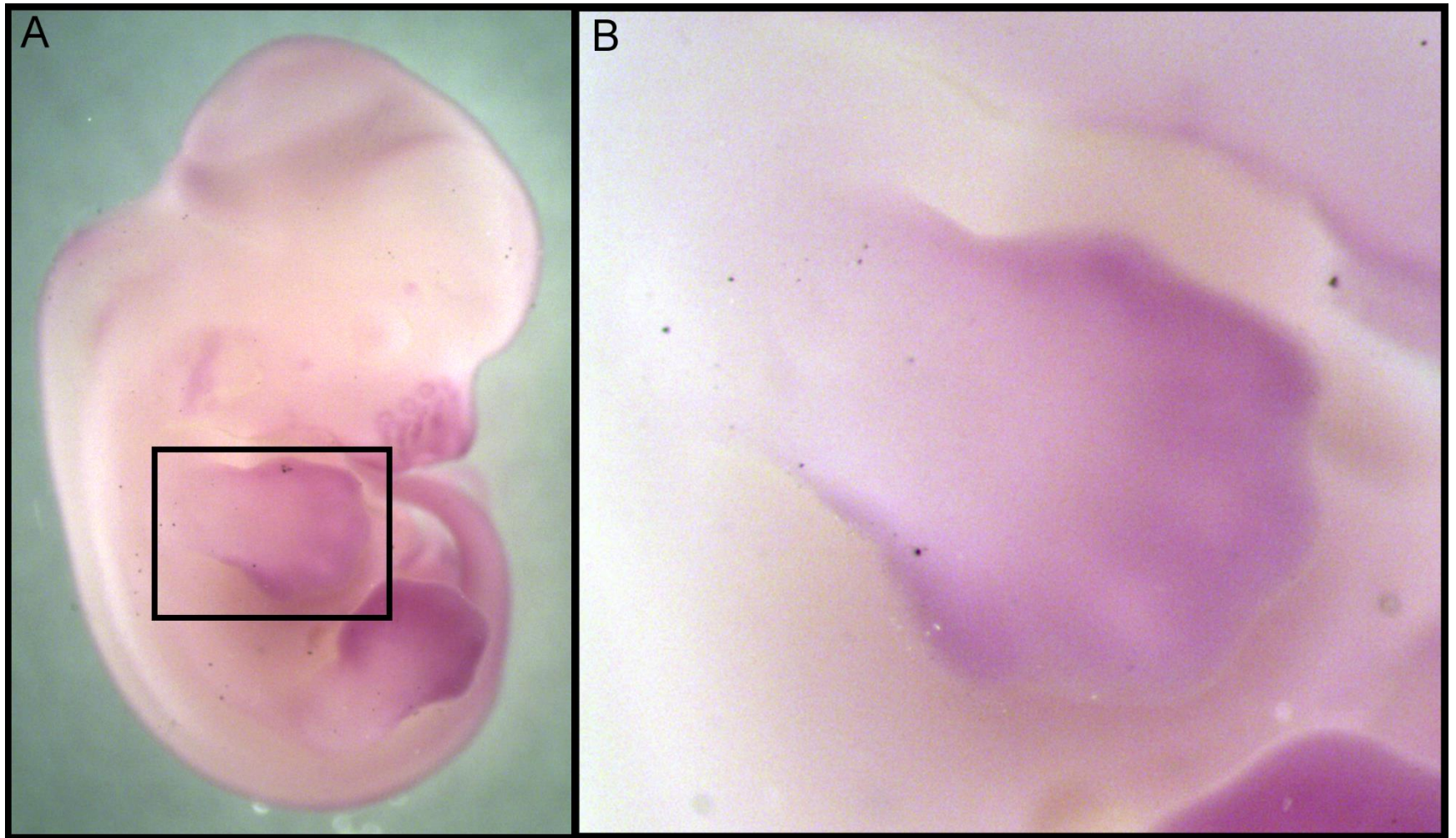


Figure 19: Embryonic Day 12.5 mouse *Cyp26b1* expression. A shows the entire embryo and black box highlights area of focus. B is the close up of the forelimb to look at forelimb expression patterns. n = 1.



Figure 20: *Carollia perspicillata* CS17 whole-mount *in situ* hybridization expression of *Cyp26b1*. n = 1.

Chapter IV

Discussion:

The goals of this study included the use of μ CT as a modern tool in developmental biology. The digital data was used to briefly describe the external, morphological development of several anatomical features throughout the 10 stages used (CS11 – 20). This data was also used to examine a coronal plane near the midline of the embryo to describe development of certain internal features. Digital data was used to focus on forelimb development in the 6 later stages (CS15 – 20), after different tissue types could be imaged. This study provides the first comprehensive volumetric assessment of tissue anatomy in a developing bat embryo. Taking advantage of the μ CT forelimb data, a potential digit patterning gene was then examined *in situ* from the stage digit condensations were first observed in the μ CT data through the stage in which the first signs of some digit identity could be observed.

The μ CT scanning worked well for all of these goals. The scanning was well suited at giving tissue level resolution within the developing embryos to identify variations in the developing tissue. The riboprobe showed specificity for the *C. perspicillata* transcript. Combined with sequence data of the riboprobe aligned with a cDNA sequence of *Cyp26b1* from *C. perspicillata*, and RNA-seq data that showed elevated levels of *Cyp26b1* in the IDM areas, we can be confident in claiming we have examined this potential digit patterning gene in a series of developing *C. perspicillata* embryos.

In this study we were able describe morphology of the developing *Carollia perspicillata* embryo with a focus on digit patterning using micro-computed tomography. We then tested the hypothesis that the spatial pattern of a digit 2 patterning candidate gene was unique in bat when compared to mouse in an attempt to validate expression differences obtained in the RNA-seq assay.

Given the initial RNA-seq data that showed highest *Cyp26b1* expression in the IDM area immediately posterior to digit 2 than other IDM areas it was appropriate to assume WISH would show a clear expression difference. Also, given the RNA-seq data, knowledge of IDM gene expression influencing final digit identity, and the altered identity of digit 2 it was reasonable to consider *Cyp26b1* as a potential digit patterning gene. However, this study was unable to show a clear difference in expression in the samples examined, although additional samples from different embryos would allow statistical testing of this result. It may not be possible to observe a difference of 2.2x using WISH. The degree of expression variation may need to be higher in order to visualize these differences.

Cyp26b1 has been shown to be critical in degrading retinoic acids and initializing chondrogenesis. The RNA-seq data suggesting a higher degree of expression in an area that influences a highly reduced digit identity is quite interesting. It seems that a higher amount of *Cyp26b1* expression would result in a higher amount of cells being recruited to take on a more distal pattern and cause more cells to enter chondrogenesis, resulting in a larger digit. Slightly larger regions of expression occurred posterior to digit 3 in the *C. perspicillata* embryos used for this study. The significance of this finding, and an explanation for the difference between the WISH data and RNAseq data requires further

study. Based on the RNAseq data, perhaps retinoic acid signaling is slightly higher in the IDM area posterior to digit 2. This would require a slightly higher amount of *Cyp26b1* and may still result in a truncated digit identity. There may also be other genes involved in the identity of this digit that play a more critical role. Given the dynamic nature of gene expression in development it seems likely that several factors are influencing digit identity and not a single gene.

Another possibility is that a higher amount of *Cyp26b1* alone is interesting, but other genes involved in the digit's identity may also be quantitatively higher. This might result in expression being negated by the relative amounts of other transcripts. One other possibility is the potential presence of non-targeted tissues may have been dissected along with the IDM areas of interest. I do not think this is the case, but it needs to be mentioned. This may result in transcripts being identified as expressed at higher frequencies than they actually are.

These findings may also indicate the RNA-seq data was inaccurate in the quantitative amount given for *Cyp26b1* in *C. perspicillata* embryos, or affected by other factors, such as differences in contribution of interdigital mesenchyme to the total interdigital tissue in the sample sequenced (ectoderm, mesoderm, vasculature, etc.). Given the known role of *Cyp26b1* in development and initiation of chondrogenesis, developmentally it makes sense that a higher degree of expression was seen posterior to a digit condensation that was longer and composed of more cellular mass. In this case, the WISH data supports an important role for *Cyp26b1* in the growth of the longest digit in the bat wing. Further, the WISH data suggests that expression of *Cyp26b1* slows earlier

in development in the IDM areas posterior to digits 1 and 2. This finding also supports the role of *Cyp26b1* expression contributing to digit lengths. Finally, when comparing *Cyp26b1* expression in mouse forelimbs to bat forelimbs at similar stages of development we saw that expression was similar in the IDM areas posterior to digits 2 and 3. In fact, in an animal for which digits of the paw are of similar length, it may make sense that expression was similar in all IDM areas.

All of these findings and potential interactions demonstrate the importance of the approach used here. Using RNA-seq alone leads to quantitative data, but not spatial expression. Using WISH alone means sorting through thousands of potential genes to examine. Using WISH to attempt to validate RNA-seq data gives you spatial expression data along with the quantitative data and is a viable approach to study genes involved in embryonic development. As we have shown, *Cyp26b1* may not play a critical role in specifying digit 2 identity, but the approach used was successful.

Traditional studies in development used external images of embryos, with a high degree of similarity to those presented here. The real advantage that was demonstrated here is the ability to re-manipulate the same data again. Once traditional imaging was performed an embryo might be preserved for some amount of time, but images at a later date may not be identical to those first taken due to aging of the sample. Using μ CT for these external images allows for revisiting the data time and again with no loss or change in the sample. If new angles of focus are needed months later the researcher has the ability to accurately capture these with confidence that the subject matter has not desiccated, discolored, over saturated, etc.

Internal sections have been included in traditional developmental studies as well. The use of μ CT to obtain the coronal planes presented above displayed some of the advantages previously mentioned. Once imaged, the data can be revisited, reimaged and manipulated to get alternative angles and sections with the confidence that the sample had not lost integrity. Other advantages were also found when imaging internal sections. Using a whole embryo, without physical sectioning, allowed for tissues to be in the undisturbed orientations they were naturally. The tissues were not cut, pulled or spatially disturbed. The internal tissues were not exposed to air so desiccation and shrinkage were minimized.

When trying to focus on a specific region of development, like forelimbs, μ CT presented more advantages. In a traditional approach there would have been a need to physically dissect each forelimb examined, image forelimbs over the rest of the body and then manipulate the images after taking them or pinning them off to the sides without damaging the tissues. μ CT assays allowed for using secondary programs to digitally section an area of interest. This allowed for visualizing tissue types only present in the area of interest, as well as measuring the change in size throughout the stages, without altering the original sample. Our volumetric dataset of 10 stages of bat embryo development provide future opportunities for digitally dissecting other developing organ systems.

As shown, μ CT as a tool in developmental assays, can be a powerful approach with many advantages over traditional methods. This study has given several examples of a novel approach to a traditional field of research. This study has only touched on

some of the advantages of μ CT as a developmental tool and we have demonstrated an important role in which the technology can be used. It is important to note, however, that there were some shortcomings in this approach.

These shortcomings included observations at very early stages of development. There may not be enough contrast difference to clearly distinguish the different tissue types that are present at these stages, potentially making it uninformative. The protocols and machine used for this study achieved 3 μ m resolutions, however this did not allow individual cells to be visualized.

In some samples there were some contrast artifacts seen in the μ CT data. These were likely particles that were trapped between wings and trunk of body that absorbed iodine. To alleviate this, I would attempt these later stages without a stabilization step. I would also attempt a more rigorous rinsing step that would just fall short of damaging the outer layer of the embryo.

The significance of WISH in this study was not the use of it, but the selection of genes used for the study. This portion of the study was aimed at describing possible digit patterning gene expression. An initial RNA-seq dataset was used to describe relative expression differences in IDM areas. Given the initial knowledge that posterior IDM areas influenced anterior digit identity, along with data showing varying amounts of IDM expression, we examined the expression of *Cyp26b1* to look for varying degrees of expression.

This study was also significant in the choice of model used. Bats have been shown to be an excellent model for developmental studies and this study focused on one

of the developmental processes that is very intriguing. Given the highly diverse nature in mammalian forelimbs and highly conservative nature of genes involved in limb patterning, using a model with highly adaptive forelimb modifications was appropriately suited for looking at digit patterning genes and other candidate digit identity genes may lead to promising results.

As this study has demonstrated it can be beneficial to revisit traditional methods with modern assays. Using new models in developmental research is also beneficial. Through this one study we have generated enough data to support many future research opportunities without exposing the samples to continuing degradation or aging. We have shown the a few of the possibilities and given suggestions for others to continue with. We have used modern approaches for assays in both μ CT and WISH that may benefit others.

Future Research Possibilities & Inquiries

Future aims for studies along these lines can include using the μ CT data to compose a thorough developmental assay of *C. perspicillata*. Along with a complete developmental assay the data can be manipulated to display the developmental origins, differentiation and refinement of several whole organs. The μ CT data can be used to measure size changes, overall volume changes and possible variations in tissue thickness throughout the developmental stages. Animations can also be made of each segmented organ or tissue changing over time through the stages.

Future aims for targeted WISH experiments include using other working riboprobes to analyze the spatial expression patterns of other candidates with quantitative expression differences (~20 total) and to compare expression patterns seen with the RNA-seq data to test whether WISH is a sensitive enough assay to verify RNA-seq data sets. Furthermore, working with developing digits and potential genetic influences to digit identities may lead to the discovery of a new signaling center at play in *C. perspicillata* embryos. Another approach to verify the possible role of potential digit patterning genes may be appropriate to use an *in ovum* approach in chick embryos, which are well suited for such analyses, to attempt to alter digit identities with the proteins that would be translated from the mRNA transcripts.

References:

- Altschul, S.F., Gish, W., Miller, W., Myers, E.W. & Lipman, D.J. (1990) "Basic local alignment search tool." *J. Mol. Biol.* 215:403-410. PubMed
- Behringer, R. R., Rasweiler IV, J. J. & Cretekos, C. J. (2009). Genetic regulation of mammalian diversity. *Cold Springs Harbor Symposia on Quantitative Biology*, LXXIV, 1-6.
- Casanova, J. C., & Sanz-Ezquerro, J. J. (2007). Digit morphogenesis: Is the tip different? *Development, Growth & Differentiation*, 49(6), 479-491
- Chen, C. H., Cretekos, C. J., Rasweiler IV, J. J. & Behringer, R. R. (2005). *Hoxd13* expression in the developing limbs of the short-tailed fruit bat, *Carollia perspicillata*. *Evolution and Development*, 7(2), 130-141.
- Cooper, L. N., Cretekos, C. J. & Sears, K. E. (2012). The evolution and development of mammalian flight. *WIREs Developmental Biology*, 1, 773-779.
- Cretekos, C. J., Wang, Y., Green, E. D., NISC Comparative Sequencing Program, Martin, J. F., Rasweiler IV, J. J. & Behringer, R. R. (2008). Regulatory divergence modifies limb length between mammals. *Genes & Development* 22, 141-151.
- Cretekos, C. J., Deng, J-M., Green, E. D., NISC Comparative Sequencing Program, Rasweiler IV, J. J. & Behringer, R. R. (2007). Isolation, genomic structure and developmental expression of *Fgf8* in the short-tailed fruit bat, *Carollia perspicillata*. *International Journal of Developmental Biology*, 51, 333-338
- Cretekos, C. J., Weatherbee, S. D., Chen, C-H., Badwaik, N. K., Niswander, L., Behringer, R. R. & Rasweiler IV, J. J. (2005). Embryonic staging system for the short-tailed fruit bat, *Carollia perspicillata*, a model organism for the mammalian order *Chiroptera*, based upon timed pregnancies in captive-bred animals. *Developmental Dynamics*, 233, 721-738.
- Dahn, R. D., & Fallon, J. F. (2000). Interdigital regulation of digit identity and homeotic transformation by modulated BMP signaling. *Science* 289(5478), 438-441.
- Dranse, H. J., Sampaio, A. V., Petkovich, M. & Underhill, M. (2001). Genetic deletion of *Cyp26b1* negatively impacts limb skeletogenesis by inhibiting chondrogenesis. *Journal of Cell Science*, 124, 2723-2734.
- Hockman, D., Cretekos, C. J., Mason, M. K., Behringer, R. R., Jacobs, D. S. & Illing, N. (2008). A second wave of *Sonic hedgehog* expression during the development of the bat limb. *PNAS*, 105(44), 16982-16987.

- Johnson, J. T., Hansen, M. S., Wu, I., Healy, L. J., Johnson, C. R., Jones, G. M., Capecchi, M. R. & Keller, C. (2006). Virtual histology of transgenic mouse embryos for high-throughput phenotyping. *PLoS Genetics*, 2(4), 0471-0477.
- Khokha, M. K., Hsu, D., Brunet, L. J., Dionne, M. S., & Harland, R. M. (2003). Gremlin is the BMP antagonist required for maintenance of Shh and Fgf signals during limb patterning. *Nature Genetics*, 34(3), 303.
- Kim, J. S., Min, J., Recknagler, A. K., Riccio, M. & Butcher, J. T. (2011). Quantitative three-dimensional analysis of embryonic chick morphogenesis via microcomputed tomography. *The Anatomical Record*, 294, 1-10.
- Lewandoski, M., Sun, X., & Martin G. R. (2000). Fgf8 signaling from the AER is essential for normal limb development. *Nature Genetics*, 26(4), 460-463.
- Mayer, F., Dietz, C. & Kiefer, A. (2007). Molecular species identification boosts bat diversity. *Frontiers in Zoology*, 4, 4.
- Metscher, B. D. (2009). MicroCT for comparative morphology: simple staining methods allow high-contrast 3D imaging of diverse non-mineralized animal tissues. *BioMed Central*, 9(11), 1-14.
- Niswander, L. (2002). Interplay between the molecular signals that control vertebrate limb development. *International Journal of Developmental Biology*, 46(7), 877-881.
- Paulus, M. J., Gleason, S. S., Kennel, S. J., Hunsicker, P. R. & Johnson, D. K. (2000). High resolution x-ray computed tomography: An emerging tool for small animal cancer research. *Neoplasia*, 2, 62-70.
- Rasweiler IV, J. J. & Badwaik, N. K. (1997). Delayed development in the short-tailed fruit bat, *Carollia perspicillata*. *Journal of Reproduction and Fertility*, 109, 7-20.
- Rasweiler IV, J. J., Cretokos, C. J., & Behringer, R. R. (2009). The short-tailed fruit bat *Carollia perspicillata*: A model for studies in reproduction and development. *Emerging Model Organisms: a laboratory manual* (537-543). Cold Springs Harbor, NY: Cold Springs Harbor Laboratory Press.
- Rennie, M. Y., Sled, J. G. & Adamson, S. L. (2013). Effects of genes and environment on the fetoplacental arterial microcirculation in mice revealed by micro-computed tomography imaging. *Microcirculation*, 21, 48-57.
- Sanz-Ezquerro, J. J., & Tickle, C. (2003). Digital development and morphogenesis. *Journal of Anatomy* 202(1) 51-58.

- Scherz, P. J., Harfe, B. D., McMahon, A. P., & Tabin, C. J. (2004). The limb bud Shh-Fgf feedback loop is terminated by expansion of former ZPA cells. *Science*, 305(5682), 396-399.
- Sears, K. E., Maier, J. A., Rivas-Astrova, M., Poe, R., Zhong, S., Kosoq, K., Marcot, J. D., Behringer, R. R., Cretekos, C. J., Rasweiler IV, J. J. & Rapti, Z. (2015). The relationship between gene network structure and expression variation among individuals and species. *PLoS Genetics*, 11(8), e1005398.
- Sekine, K., Ohuchi, H. Fujiwara, M., Yamasaki, M., Yoshizawa, T., Sato, T...Kato, S. (1999). Fgf10 is essential for limb and lung formation. *Nature Genetics* 21(1), 138-141.
- Sun, X., Mariani, F. V., & Martin, G. R. (2002). Functions of FGF signaling from the apical ectodermal ridge in limb development. *Nature*, 418(6897), 501.
- Suzuki, T. (2013). How is digit identity determined during limb development? *Development, Growth & Differentiation*, 55(1), 130-138.
- Verheyden, J. M., & Sun, X. (2008). An Fgf/Gremlin inhibitory feedback loop triggers termination of limb bud outgrowth. *Nature*, 454(7204), 638-641
- Wada, N., Kawakami, Y., & Nohno, T. (1999). Sonic hedgehog signaling during digit pattern duplication after application of recombinant protein and expressing cells. *Development, Growth & Differentiation*, 41(5), 567-574.
- Wing, D. W., Spring, S. & Henkelman, R. M. (2013). Structural stabilization of tissue for embryo phenotyping using micro-CT with iodine staining. *PLoS ONE*, 8(12), 1-7.
- Yashiro, K., Zhao, X., Uehara, M., Yamashita, K., Nishijima, M., Nishino, J., Saijoh, Y., Sakai, Y. & Hamada, H. (2004). Regulation of retinoic acid distribution is required for proximodistal patterning and outgrowth of the developing mouse limb. *Developmental Cell*: 6, 411-422.
- Zheng Zhang, Scott Schwartz, Lukas Wagner, and Webb Miller (2000), "A greedy algorithm for aligning DNA sequences", *J Comput Biol* 2000; 7(1-2):203-14.

Appendix:



CS11.mov



CS11.mp4



CS12.mov



CS12.mp4



CS13.mov



CS13.mp4



CS14.mov



CS14.mp4



CS15.mov



CS15.mp4



CS16.mov



CS16.mp4



CS17.mov



CS17.mp4



CS18.mov



CS18.mp4



CS19.mov



CS19.mp4



CS20.mov



CS20.mp4